ELSEVIER

Contents lists available at ScienceDirect

Earth-Science Reviews

journal homepage: www.elsevier.com/locate/earscirev





Mesozoic intraplate tectonism of East Asia due to flat subduction of a composite terrane slab

Liang Liu^{a,b,c}, Lijun Liu^{a,*}, Yi-Gang Xu^{b,c,*}

- ^a Department of Geology, University of Illinois at Urbana-Champaign, USA
- ^b State Key Laboratory of Isotope Geochemistry, Guangzhou Institute of Geochemistry, Chinese Academy of Sciences, Guangzhou, 510640, China
- ^c CAS Center for Excellence in Deep Earth Sciences, Guangzhou, 510640, China

ARTICLE INFO

Keywords: Flat subduction Terrane accretion Intraplate magmatism Yanshanian Orogeny

ABSTRACT

The widespread Middle Jurassic to Early Cretaceous (J2-K1) intraplate tectonism of East Asia has recently been proposed to reflect the flat subduction of the Izanagi plate, whose mechanism, however, remains poorly constrained. Here, we compare these geological records with those within the western United States (U.S.) during the Laramide flat subduction. Two prominent differences are identified during slab advance: 1) western U.S. witnessed continental-scale subsidence and marine inundation, while East Asia experienced mostly basin inversion implying uplift; 2) the landward migrating magmatism in western U.S. quickly evolved into a regional magmatic lull that lasted for >40 Myr, but the East Asian magmatism was largely continuous in space and time. Assisted with numerical models, we show that a flat slab could indeed reproduce the observed East Asian crustal deformation and topographic history during the advance and retreat of the slab. We further find that 1) this slab should be more buoyant than the Laramide slab so that the former oceanic slab could break off which led to surface uplift instead of subsidence, and 2) the crust of the flat slab melted more easily than an oceanic one. The observation that the J2-K1 tectonism was largely contemporary with the assembly (ca. 180-137 Ma) of exotic terranes along the east coast implies that the flat sab underplating North China and Northeast China likely represented subduction of the buoyant continental lithosphere associated with these terranes. The terrane slab could have carried and flattened portions of the nearby oceanic slab with it, forming a giant composite flat slab that defined the J2-K1 intraplate tectonism within East Asia.

1. Introduction

The Middle Jurassic to Early Cretaceous tectonism of East Asia is characterized by extensive magmatism and crustal deformation across >1000 km wide inland areas (Fig. 1), intervened by two regional unconformities preserved in North China at ca. 165 and 140 Ma, respectively (Fig. 2) (Wong, 1927, 1929;Davis et al., 1998;Meng, 2017;Davis and Darby, 2010;Huang, 2015;Dong et al., 2018;Wu et al., 2019). Key tectonic processes include 1) moderate crustal shortening (Meng, 2017; Davis et al., 1998;Davis and Darby, 2010;Wu et al., 2019;Zhu and Xu, 2019) and inboard migration of predominant adakitic magmatism due to deep crustal melting (ca. 165–140 Ma) (Gao et al., 2004;Xu et al., 2008;Ma et al., 2012, 2015), and 2) severe crustal extension (Davis and Darby, 2010;Li et al., 2019;Wu et al., 2019;Zhu and Xu, 2019) and oceanward migration of magmatism with an increasing asthenospheric signature (140–110 Ma) (Xu, 2001;Xu et al., 2009;Zheng et al., 2018).

After the Late-Jurassic (*J2*) regional unconformity (ca. 165 Ma) (Fig. 2), localized basins within East Asia started to receive terrestrial sediments, ~20 Myr earlier than those further east (Figs. 1b, 2) (Liu et al., 2017; Meng, 2017; Wu et al., 2019; Zhu and Xu, 2019; Li et al., 2019). In contrast, following the subsequent Early Cretaceous (*K1*) unconformity (ca. 140 Ma), widespread extensional basins (Songliao, Huabei-Bohai Bay & South Yellow Sea) developed almost synchronously, bounded by many left-lateral strike-slip faults (Liu et al., 2017; Li et al., 2019; Wu et al., 2019; Zhu and Xu, 2019) (Figs. 1a & 2). This history of intraplate activities is conventionally called the Yanshanian Orogeny, initially named in the Yanshan region of North China (Wong, 1927, 1929), but then widely referred to as a specific geological period (ca. 180–110 Ma) when active tectonism occurred across a much larger area of East Asia (Figs. 1–3) (Wong, 1927, 1929; Zhou and Li, 2000; Wu et al., 2011; Davis and Darby, 2010; Dong et al., 2018; Wu et al., 2019).

By the end of Early Jurassic (ca. 200-180 Ma), collisional orogenesis

E-mail addresses: ljliu@illinois.edu (L. Liu), yigangxu@gig.ac.cn (Y.-G. Xu).

^{*} Corresponding authors.

surrounding the North China block came to an end (Yin and Nie, 1993; Li, 1994; Gao et al., 1995; Meng and Zhang, 1999; Xiao et al., 2003; Li et al., 2014). Since then, the Izanagi Plate started to subduct along the east coast (Wu et al., 2011; Wu et al., 2019; Zhu and Xu, 2019). Shortly after, during the period of ca. 180-137 Ma, an enormous volume of continental terranes accreted onto East Asia (Khanchuk et al., 2016;Liu et al., 2017;Zhou and Li, 2017;Li et al., 2019;Zhu and Xu, 2019;Wu et al., 2011; Wu et al., 2019) (Fig. 1a). Although spatially distributed today, their consistent age and rock types suggest that these terranes could have been a coherent lithospheric block during the Mesozoic (Isozaki et al., 2010;Kabir et al., 2018;Khanchuk et al., 2016;Liu et al., 2017;Li et al., 2019;Matsukawa et al., 2005;Zhou and Li, 2017;Wu et al., 2011). This history of terrane accretion overlapped with the early part of the Yanshanian tectonism (ca. 165-110 Ma). A causal relationship between the two has not been previously identified, but it is a salient point we attempt to make by presenting this review.

The two stages of the Yanshanian tectonism were coeval with a succession of landward and oceanward magmatic migration, respectively, where the most prominent inland migration (up to 1500 km from the present-day trench location) occurred between $45^{\circ}N$ - $35^{\circ}N$, reaching as far as ~114°E (Fig. 3). However, on the south between $35^{\circ}N$ and $25^{\circ}N$, only the trench-ward magmatic migration can be identified (Fig. 3d). Beyond the above region (north of $45^{\circ}N$ and south of $25^{\circ}N$), the magmatic arc was rather stationary, without obvious trench-perpendicular migration (Fig. 3b and e). Among these massive eruptions of dominantly felsic magmatism (ca. 180-110 Ma), the most migratory ones were adakitic granitoids commonly interpreted as due to deep melting of ancient continental crust (Gao et al., 2004;Xu et al., 2008;Ma et al., 2012, 2015;Zhang et al., 2010a).

Many mechanical models have been proposed to explain the J2-K1 tectonism, with a particular focus on the region of the North China Craton. Specifically, the intraplate magmatism (Fig. 3) has been attributed to modification/reworking of the cratonic/orogenic lithosphere through lower crustal delamination that was caused by surrounding continental collision (Gao et al., 2004;Xu et al., 2008;Xu et al., 2009;Liu et al., 2008a), thermo-mechanical erosion (Xu, 2001; Meng, 2017),

mantle re-hydration (Niu, 2005), mantle refertilization/rejuvenation (Zhang et al., 2008;Yang et al., 2008;Zheng et al., 2018;Zheng and Dai, 2018;Wu et al., 2019), lithospheric delamination triggered by low-angle subduction (Zhang et al., 2010b), or by surrounding orogenesis (Liu et al., 2018a;Liu et al., 2018). Note that, these earlier models mostly focused on the origin of localized magmatism, where the spatial-temporal migration of the J2-K1 magmatism (Figs. 3, 6) were largely overlooked.

Regarding the multiple episodes of Yanshanian crustal deformation (Figs. 1-2), previous studies usually referred to changes in the subduction direction of the Izanagi plate as the dominant reason (Wu et al., 2008; Xu et al., 2009; Windley et al., 2010; Zhu et al., 2012; Kusky et al., 2014; Zheng et al., 2018; Dong et al., 2018), while some workers highlighted the role of much earlier collisions between the North China and South China blocks (Menzies et al., 2007) and/or that between the North China and Siberian blocks (Meng, 2003; Davis and Darby, 2010). According to recent plate reconstructions, the subduction direction of Izanagi plate gradually changed from northwest to west during the Middle Jurassic and Early Cretaceous, during which East Asia mostly drifted along the north-south direction (Isozaki et al., 2010; Müller et al., 2016, 2019; Liu et al., 2017). These processes might indeed have caused some variations in the plate boundary interaction, in line with previous propositions (Wu et al., 2008; Xu et al., 2009; Zhu et al., 2012; Zheng et al., 2018). However, plate motion change and reorganization are common both regionally and globally, but only very few places experienced intense intraplate tectonism as that observed in the J2-K1 East Asia. Regarding the role of continental collision as noted above, first, the amalgamation between the North China and surrounding blocks finished no later than Late Triassic (ca. 210 Ma), much earlier than the initialization of the J2-K1 tectonism (ca. 180 Ma) (Figs. 1-3) (Wu et al., 2008, 2011; Xu et al., 2009; Wu et al., 2019; Zhu and Xu, 2019). Second, the earlier collisional orogenesis should have led to mostly north-south oriented deformation, but most of the J2-K1 magmatism and crustal deformation in East Asia followed a dominantly east-west direction (Figs. 1–3). Consequently, mechanisms other than plate kinematics and continental collision must be present during the large-scale J2-K1

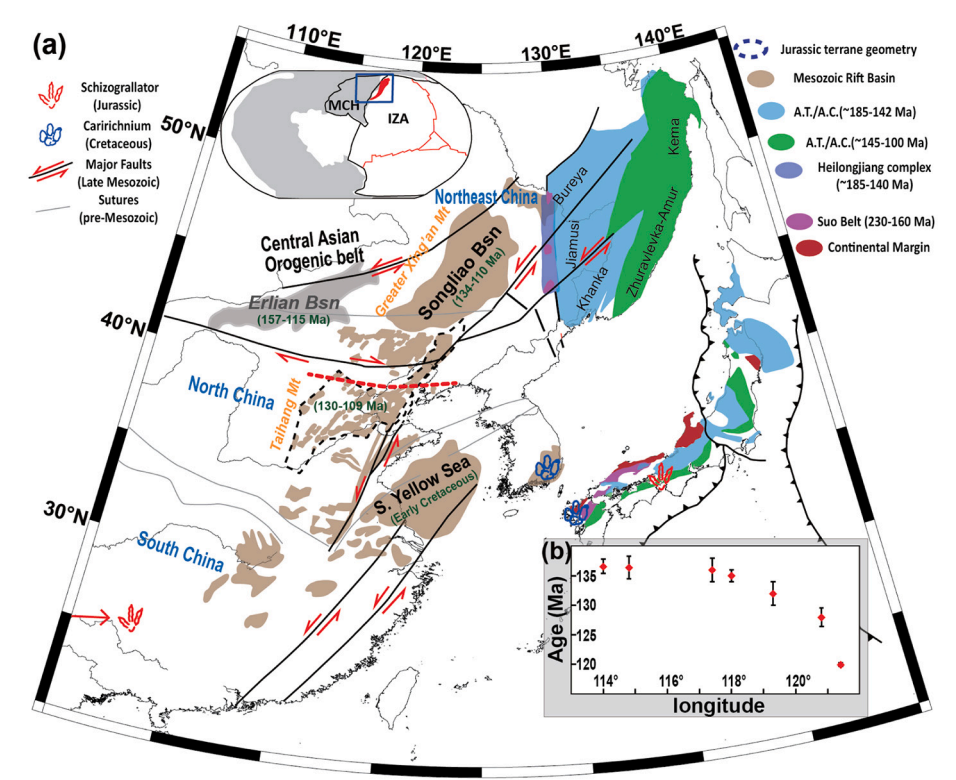


Fig. 1. Major tectonic features of late Mesozoic Eastern Asia. (a) Grey and brown regions represent Mesozoic rifting basins. In North China, densely distributed Cretaceous relic depocenters are preserved. Due to significant Cenozoic extension and sedimentation (Li et al., 2019; Liu et al., 2017; Wu et al., 2019; Zhu and Xu, 2019), the specific range for the Mesozoic basin(s) in North China is hard to determine. The thin black dashed line marks the range of the Cenozoic Bohai Bay Basin developed upon the Cretaceous one(s). The information regarding the ichnofossils and the ages of continental terranes & accretionary complexes is based on several previous studies (Isozaki et al., 2010; Kabir et al., 2018; Khanchuk et al., 2016; Liu et al., 2017; Li et al., 2019; Matsukawa et al., 2005; Zhou and Li, 2017; Wu et al., 2011). The thumbnail demonstrates the reconstructed location of the proposed continental terrane(s) at ca. 160 Ma relative to the Mongolia-China (MCH) Izanagi (IZA) plates (Liu et al., 2017; Li et al., 2019). (b) The onset time of Earth-Cretaceous sedimentation in North China, along the east-west profile illustrated by the red dashed line in a (Wu et al., 2019; Zhu and Xu, 2019). (For interpretation of the references to colour in this figure legend, the reader is referred to the web version of this article.)

magmatism and crustal deformation within East Asia.

Most recently, the migratory Yanshanian magmatism was interpreted as reflecting the formation of a flat slab from the subducting Izanagi Plate beneath East Asia (Zheng et al., 2018;Li et al., 2019;Wu et al., 2019; Zhu and Xu, 2019). This is similar to the initial inference of Farallon flat subduction (Coney and Reynolds, 1977) associated with the Laramide Orogeny (ca. 80–40 Ma), an intraplate orogenic event within the western United States (U.S.). In both cases, a critical observational constraint is the landward migrating magmatism (Henderson et al., 1984; Humphreys, 1995; Saleeby, 2003; DeCelles, 2004; Liu et al., 2010; Heller and Liu, 2016). In order to further understand this new interpretation of the Yanshanian magmatism, especially the underlying mechanism that is still poorly constrained, we provide a detailed comparison between the East Asian intraplate tectonism and that occurred during the Laramide orogeny within the western United U.S. By considering their similarities and differences, together with quantitative numerical modeling, we aim at a better understanding of their respective mechanisms of flat-slab subduction.

In Section 2, through a direct comparison with the flat-slab-related geological records within western U.S., we summarize the distinctive and diagnostic tectonic features for the East Asian flat subduction. In Section 3, using numerical simulations, we quantitatively analyze the underlying geodynamics of the unique East Asian tectonism. Relative to the Laramide-style flat subduction, we arrive at an alternative model: the J2-K1 flat slab below East Asia could have resulted from the subduction of continental lithosphere during the process of terrane accretion along the east coast. We suggest that the buoyant continental flat slab could carry and flatten its surround oceanic slab, such as that below South China, ultimately creating a composite flat slab beneath East Asia during ca. 180–140 Ma.

2. Flat-slab related tectonism in East Asia and western U.S.

Flat slab subduction could significantly affect the geology of the overriding continental plates (Cawood et al., 2009; Kapp and DeCelles, 2019), with typical examples including the Laramide orogeny in the

western U.S. (Saleeby, 2003; Liu et al., 2010; Heller and Liu, 2016) and the J2-K1 tectonism in East Asia (Figs. 1 and 3; Wu et al., 2019). A detailed review and comparison of the geological records in both these regions can help us to better understand the nature and consequences of these abnormal subduction scenarios. In the following, we mainly focus on the spatial and temporal distribution of surface topography (uplift or sedimentation) and intraplate magmatism, both of which are taken as the most relevant surface responses of flat subduction (Saleeby, 2003; Liu et al., 2010; Heller and Liu, 2016; Wu et al., 2019). For convenience, we will use "Laramide flat subduction (slab)" to represent the Late Cretaceous- Cenozoic flat subduction (ca. 90–50 Ma) beneath western U. S., and "Yanshanian flat subduction (slab)" to represent the Middle Jurassic -Early Cretaceous flat subduction (ca. 180–140 Ma) beneath East Asia.

2.1. Topographic responses during flat-slab subduction

As discussed above, in East Asia, during the inboard migration of the Yanshanian flat slab (ca. 180–140 Ma), majority of the sedimentary basins above experienced an inversion, recorded as the regional unconformity at ca. 165 Ma (Fig. 2) (Meng, 2017; Meng et al., 2019; Liu et al., 2019a; Wu et al., 2019). Before and after this unconformity, only terrestrial and volcanic sediments are identified in basin accumulates (Fig. 2), indicating a predominantly terrestrial (or subaerial) environment (Meng, 2017; Meng et al., 2019; Liu et al., 2019b; Wu et al., 2019).

Accompanying the subsequent retreat of the Yanshanian flat slab during the Early Cretaceous, widespread crustal extension and sedimentation occurred (Fig. 1). The dominant rifting basins suggest an important topographic contribution from isostatic subsidence due to crustal thinning. Sediments within these basins are terrestrially sourced as well (Fig. 2). This indicates that surface subsidence caused by the underlying flat slab was mostly local in scale and that continental East Asia was most likely not subsiding to below sea level during this time.

For comparison, the paleogeography of the western U.S. from the Early Cretaceous is illustrated in Fig. 4. At \sim 120 Ma, prior to the Laramide flat slab, the interior of western U.S. was dominated by

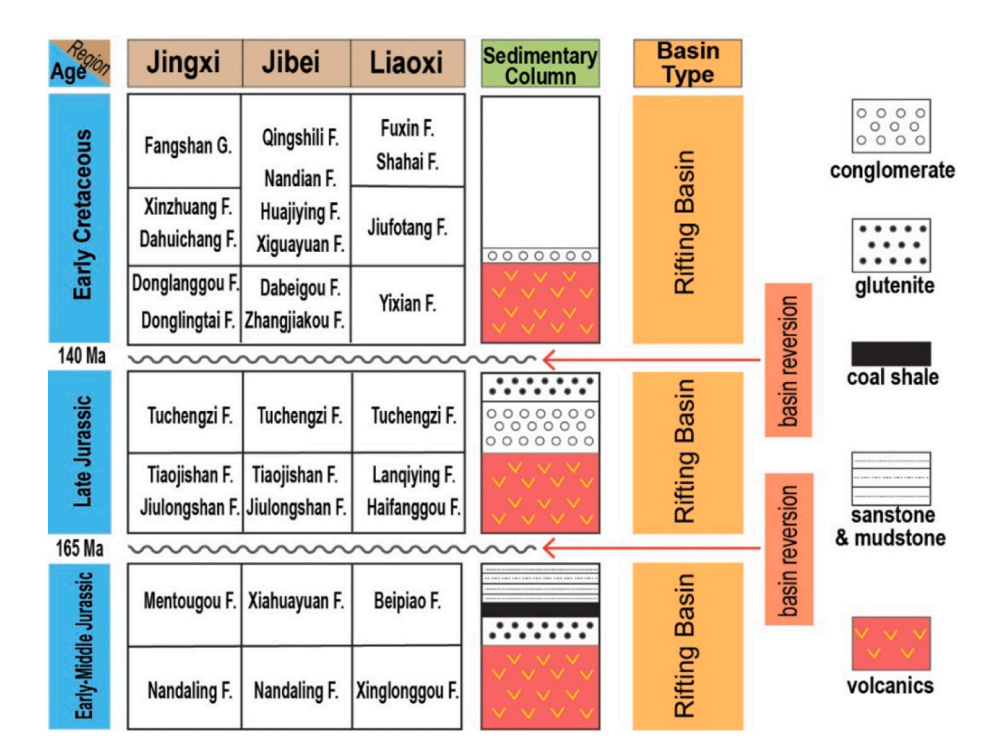


Fig. 2. Mesozoic stratigraphy in North China characterizing Yanshanian tectonism (after Meng, 2017). Two regional sedimentary unconformities are recorded in the remained Mesozoic basins, separately in ca. 165 and 140 Ma. G.-Group. F.-Formation.

contractional deformation, mainly accepting terrestrial sediments off the west coast (Fig. 4a). As the flat slab moved inboard (ca. 90–60 Ma) (Liu et al., 2010;Heller and Liu, 2016), regions east of Sevier belt started to subside and experienced widespread marine transgression; this eventually formed the Western Interior Seaway (WIS), whose maximum spatial extent occurred around 80 Ma (Fig. 4b) with \sim 1 km of tectonic subsidence, much larger than the amplitude of sea level fluctuations (Liu et al., 2011). This episode of surface subsidence was interpreted as due to the downward viscous pull (e.g., dynamic subsidence) from the sinking oceanic Farallon slab below the region (Fig. 4b) (Liu et al., 2008b;Liu, 2015). This interpretation is further supported by the flat-lying WIS strata deposited above much of the cratonic platform (Liu et al., 2011) indicating little contribution from crustal deformation.

The WIS is also characterized by progressive eastward migration of depocenters (Liu et al., 2011; Chang and Liu, 2019, 2020), following the landward migrating dynamic subsidence (Heller and Liu, 2016). The WIS largely ended by ~60 Ma (Fig. 4c), after which both dynamic uplift (e.g., Liu et al., 2010) and isostatic uplift (e.g., Roy et al., 2009) raised the topography to the present-day high elevation (Fig. 4d). The Cenozoic uplift history of the western U.S. largely coincided with the demise and/or retreating of the former flat slab (Fig. 4; Humphreys, 1995; Heller and Liu, 2016).

In comparison, the East Asian Yanshanian flat slab and the western U.S. Laramide flat slab led to an opposite pattern of topographic response. The former caused earlier uplift and later subsidence of inland areas during the advance and retreat of the flat slab, respectively; significant crustal deformation resulted that also contributed to the topographic evolution. The latter, however, caused earlier subsidence and later uplift, with much less crustal thickness change throughout the flat slab cycle. These contrasting properties of topographic expression suggest that the Yanshanian flat slab and Laramide slab may have been formed from different mechanisms. The general consensus that the Laramide events resulted from the flat subduction of the Farallon slab (Coney and Reynolds, 1977;Tarduno et al., 1985;Saleeby, 2003;Liu et al., 2010;Heller and Liu, 2016) indicates that the Yanshanian events require a mechanism that is tectonically different from a pure oceanic flat slab.

(b) 200 N = 679N = 283180 160 g 140 age 120 Age 120 Age 1 100 80 80 2000 1500 1000 500 Distance (km) 1500 1000 500 Distance (km) 0 -500 2000 -500 (a) (d) 200 180 160 140 e 120 e (b) 100 80 (c) 1000 500 Distance (km) 2000 1500 -500 (e) 200 N = 753180 160 140 120 100 80 2000 1500 1000 500 Distance (km)

2.2. Spatial and temporal distribution of intraplate magmatism

Landward migration of arc magmatism has been widely used to suggest the reduction of slab dip angle, with the extreme case being flat-slab subduction, such as that happened within both the western U.S. (e. g., Coney and Reynolds, 1977) and East Asia (Wu et al., 2019). Here we take a close look at these two scenarios, during which we evaluate the similarities and differences between their spatial and temporal patterns. The data for western U.S. magmatism is from the NAVDAT repository (NAVDAT.org).

For the case of western U.S. (Fig. 5), the temporal evolution during ca. 90–20 Ma between 50°N and 34°N (Fig. 5b, c), the typical time and location for the Laramide slab (Saleeby, 2003;Liu et al., 2010), is similar to that observed in the region between 35°N and 25°N within East Asia (Fig. 3d), where only the late-stage trench-ward migration of magmatism can be identified. This is in contrast to the magmatic evolution between 45°N and 35°N in East Asia (Fig. 3c), where an obvious early landward migration is also present (Fig. 3b). As shown later (Figs. 6, 8), this missing branch within the otherwise continuous magmatic trend represents a gap both in space and time, a feature termed *magmatic lull* (e.g., Henderson et al., 1984).

Besides the regionalized temporal patterns as discussed above (Figs. 3 & 5), we further analyze the detailed spatial-temporal evolution of the magmatic records for both East Asia (Figs. 6 & 7) and western U.S. (Figs. 8 & 9). To associate the magmatism with the underlying flat slabs, we refer to recent studies for the plausible geometry of these slabs. In the case where detailed evolution of slab configuration is unavailable, such as the Yanshanian flat slab due to still limited research, we combine surface tectonism including the magmatic front (see definition in the caption of Fig. 6), crustal deformation (Fig. 1) and petrologic constraints (Zheng et al., 2018;Liu et al., 2019a) to outline the possible spatial extents of the slab (Fig. 6).

According to the available data in East Asia, during the landward migration of the Yanshanian flat slab (ca. 180–140 Ma, Fig. 3c), the trench-parallel extent of magmatism also gradually extended (Fig. 6a–d). The magmatic records in SLB (Songliao basin) and BBB (Bohai Bay Basin) regions, due to the thick Mesozoic and Cenozoic sediment cover (Liu et al., 2017; Zhi-qiang et al., 2010), are unavailable, thus forming two apparent gaps. In the region above the flat slab, approximated as the area from the magmatic front to the trench,

Fig. 3. Magma distribution of Late Mesozoic East Asia. (a) Map distribution of the J2-K1 magnetism (Niu et al., 2015; Wu et al., 2007; Zhai et al., 2016; Kim et al., 2015). Trench position is based on the distribution of continental blocks in Fig. 1a and Wu et al., 2019. (b-e) Magma ages plotted against distance from the trench within four latitudinal bands shown in a (see Fig. S1 for the magma ages plotted against longitude). Distance is calculated from the nearest Jurassic trench, with positive distance being west and negative east. The cyan dashed contours in c and d roughly mark the distribution of the adakitic rocks. The grey dashed line marks spatial-temporal range lacking magmatic records. Jm- Jiamusi terrane. Kh- Khanka terrane. By- Bureya terrane. (For interpretation of the references to colour in this figure legend, the reader is referred to the web version of this article.)

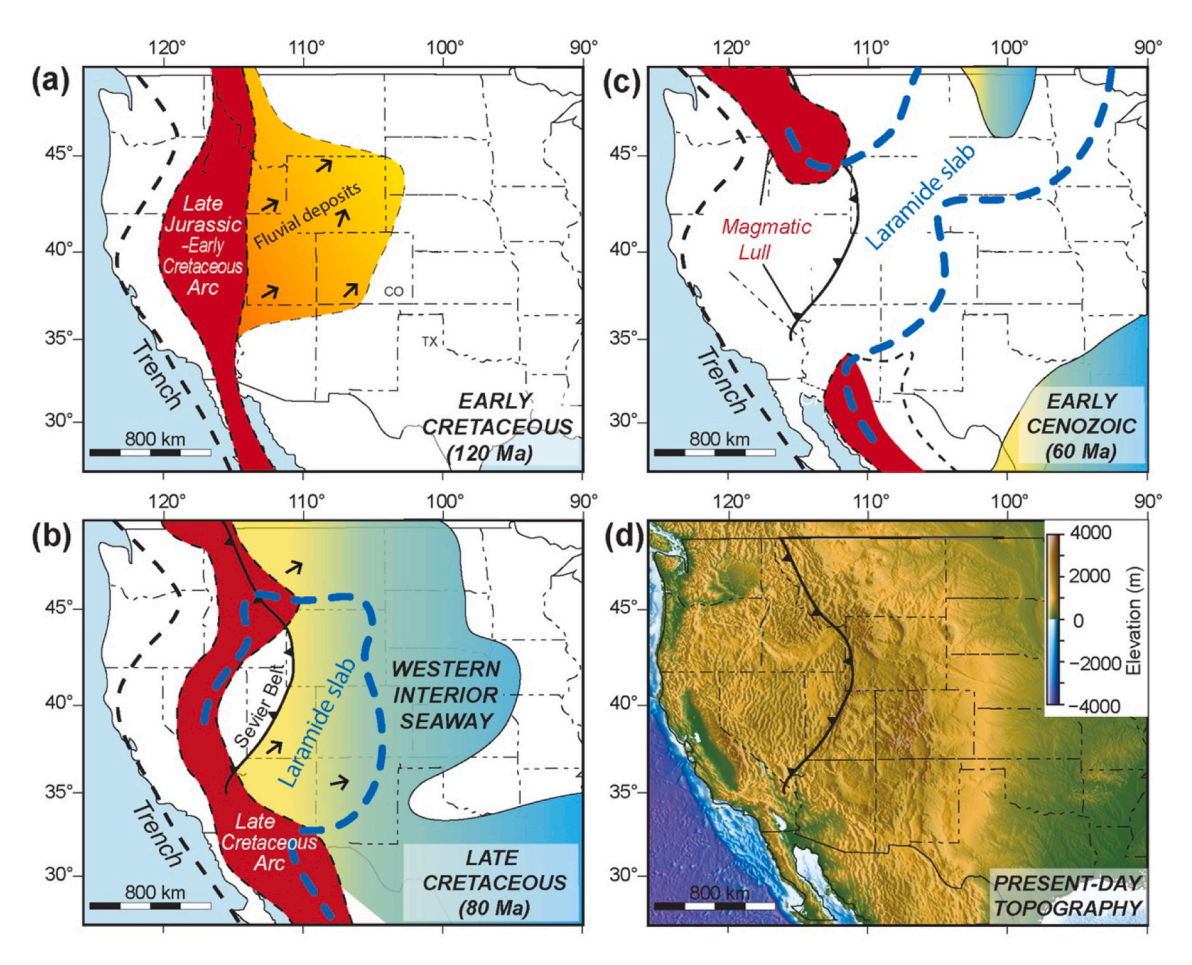


Fig. 4. Paleogeography of Western U.S since the Early Cretaceous (based on Heller and Liu, 2016). (a) In the Early Cretaceous, arc magmatism focused along the continental margin. Fluvial conglomerate deposits (the orange shading) are found within the continental interior. (b) In the Late Cretaceous, arc magmatism migrates landward with a magmatic lull formed above the flat slab (Liu et al., 2010). The continental interior east of the Sevier belt experienced widespread marine transgression. (c) By the earliest Cenozoic, the magmatic lull fully developed and marine inundation largely disappeared due to surface rebound. (d) Surface uplift continued during the Cenozoic to reach the present high topography of the western U.S. Note that little crustal extension occurred east of Sevier during the Cenozoic demise of the Laramide slab. This feature contrasts with the extensive Early-Cretaceous crustal extension in East Asia during the detachment of the Yanshanian flat slab.

magmatism had remained mostly active, except for SLB and BBB where data are not available (Fig. 6a–d).

As the flat slab reached its maximum inland extent between ca. 150 and 140 Ma, magmatism seemed to be restricted to within a relatively narrow belt along the magmatic front (Fig. 6e). This brief (<10 Myr) period of attenuating intraplate magmatism (a magmatic gap according to Wu et al., 2007 and Xu et al., 2009) is also visible in the magmatic "flux" approximated using the number density of rock samples (Fig. 7). Since ca. 140 Ma, intraplate magmatism intensified in the region above the slab (Fig. 6f), and this was interpreted as a result of the flat slab being detached from the base of the upper plate (Wu et al., 2019). Between ca. 130 and 110 Ma, the most intense magmatism gradually shifted towards the trench. During this period, the recorded magmatic flux also reached the peak value (Figs. 6g, h, 7).

For the case of western U.S., the landward motion of the Laramide flat slab during ca. 90–50 Ma (Liu et al., 2010; Heller and Liu, 2016) was also accompanied by obvious inboard migration of the magmatic arc in regions north of ~42°N and south of ~32°N (Fig. 8b–f). However, between 42°N and 32°N, the magmatic arc mostly waned over time and largely disappeared by 70 Ma, forming a regionally extensive magmatic lull (Henderson et al., 1984). Within this region, from 80 Ma to 40 Ma, only very sparse magmatism appeared (Fig. 8c–f). Within this broad amagmatic region, a magmatic island on the front edge of the flat slab (Liu et al., 2008a) had kept active till 20 Ma or later (Fig. 8b–f), whose

Cretaceous appearance formed the Colorado Mineral Belt with subsequent volcanism mostly involving melting of the continental crust (Chapin, 2012). This feature might be initially caused by some slab window within the flat slab, such as that proposed within the Nazca slab (Hu and Liu, 2016) and the Juan de Fuca slab (Zhou et al., 2018). Discounting this magmatic island as being typical arc magmatism results in a distinct period of magmatic quiescence that lasted for \sim 40 Myr (Fig. 9b)

Starting as early as 50 Ma, magmatism started to reappear locally within the region of the previous magmatic lull (Fig. 8f), and strongly intensified by ca. 40–30 Ma (Fig. 8g). This resulted in a rapid surge of the magmatic intensity (Fig. 9b). According to Humphreys (1995), these Cenozoic magmas formed mostly around the rim of the retreating flat slab segment (Fig. 8f–h). This magma-slab relationship is the same as that during the advance of the Laramide slab (Fig. 8b–e). Furthermore, we note that a prominent magmatic lull above a flat oceanic slab, as that observed in the western U.S., was also observed during the late-Cenozoic Yakutat flat slab subduction in southern Alaska (Finzel et al., 2011) and the ongoing Peruvian and Chilean flat slabs in South America (Gutscher et al., 1999).

Comparatively, the Laramide magmatic lull is much more prominent, both spatially (much of the western U.S.) and temporally (from 90 to 20 Ma), than that observed associated with the Yanshanian flat slab (a brief 10 Myr window). Another important difference is that continuing

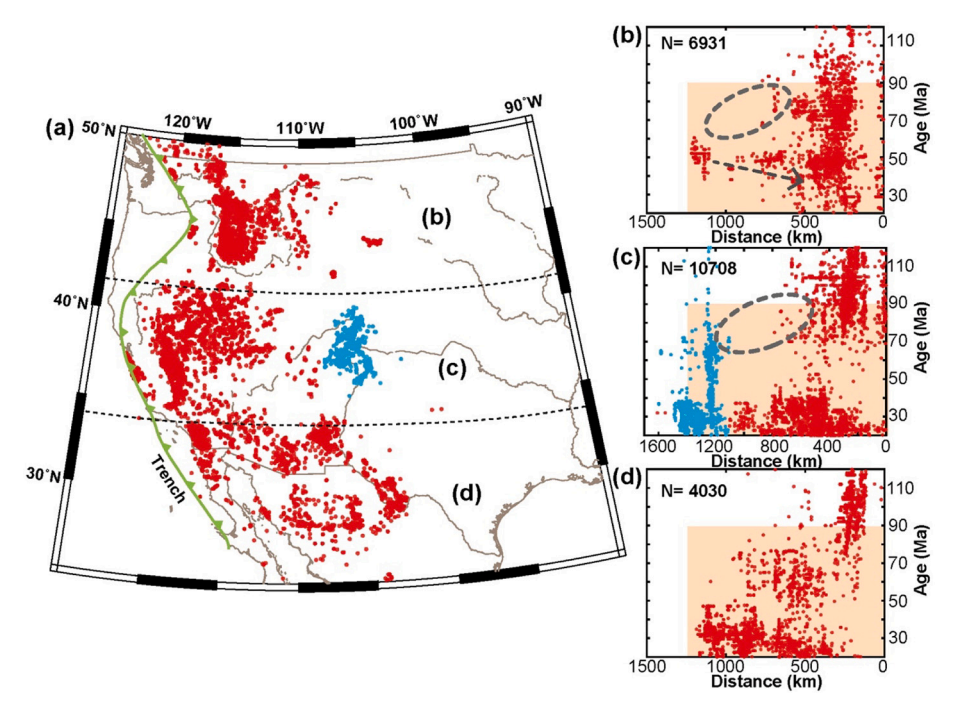


Fig. 5. Magmatism in western U.S. between 120 and 20 Ma. (a) Distribution of magmas in a map view (data are download from www.navdat.org). Each red dot marks one sample. Blue dots represent magmas associated with the Colorado mineral belt. The trench position is for Late Cretaceous time, based on Heller and Liu (2016). (b-d) Magma age plotted against distance from the trench within three latitudinal bands shown in a (50–41°N, 41–34°N and 34–25°N). The grey dashed circles outline the magmatic lull range of the Laramide flat slab (Liu et al., 2010; Heller and Liu, 2016). (For interpretation of the references to colour in this figure legend, the reader is referred to the web version of this article.)

magmatism mostly occurred around the edge of the Laramide flat slab, leaving the area above the flat slab largely amagmatic throughout the entire time since 90 Ma (Figs. 8, 9). In a sharp contrast, magmatism spatially (Fig. 6) and temporally (Fig. 7) sustained above the Yanshanian slab.

As a summary of Sections 2.1 and 2.2, several major differences exist between the Laramide and Yanshanian flat slabs. To reiterate, the East Asian intraplate deformation during the Yanshanian flat-slab cycle is characterized as two phases of regional uplift followed by extensive crustal extension and subsidence (Figs. 1, 2), while western U.S. first experienced moderate Laramide crustal shortening and coeval, wide-spread surface subsidence, followed by continental-scale uplift (Fig. 1 vs. Fig. 4). In terms of the magmatic evolution, the Laramide arc waned as it migrated inland to eventually formed a magmatic lull above the flat slab; this is opposite to the overall sustaining Yanshanian magmatism in East Asia (Figs. 3, 5–9). We suggest that these differences are mechanistically significant to imply that the oceanic flat-slab model that explains the Laramide tectonism may not work for the Yanshanian tectonism in East Asia.

Besides the implication from surface tectonics as discussed above, the occurrence of an oceanic (Laramide-style) flat slab beneath Mesozoic East Asia also seems to be questionable. The two main mechanisms for flat slab formation include: 1) fast moving overriding-plate (e.g., van Hunen et al., 2004;Liu and Currie, 2016) and 2) a buoyant subducting slab (van Hunen et al., 2000, 2002). Regarding mechanism 1, the Mesozoic motion of the Eurasian plate (Müller et al., 2016;Liu et al., 2017) was much smaller than necessary for flat-slab formation (van Hunen et al., 2002, 2004;Liu and Currie, 2016). Regarding mechanism 2, the reconstructed Izanagi plate during the Jurassic was old (>80 Myr) (Liu et al., 2017;Müller et al., 2016, 2019), thus disfavoring slab flattening due to seafloor age (Hu et al., 2016;van Hunen et al., 2002; van Hunen et al., 2004). Consequently, additional sources of slab buoyancy were required.

Based on the above reasoning, we further consider the geodynamics of flat slab formation due to subduction of an overall buoyant downgoing plate, as is the focus of the following section. We will utilize numerical simulations to quantitatively illustrate the key geodynamic properties. We first evaluate if such a flat slab could cause the Yanshanian crustal deformation observed in East Asia (Figs. 1–2). Then we

try to pin down the appropriate geodynamic conditions that can explain the different characteristics of magmatism and crustal deformation between East Asia and western U.S.

3. Geodynamics of East Asian flat subduction

We use a MATLAB-based software package to carry out 2-D numerical experiments (Liu et al., 2018a;Liu et al., 2018). This package is based on the Lagrange-type finite element code MILAMIN (Dabrowski et al., 2008). It has a free-surface boundary condition (Andrés-Martínez et al., 2015) and have been benchmarked with a study of free subduction (Liu et al., 2018a). A triangular mesh is adaptively generated/regenerated according to the distribution of materials on tracers (Liu et al., 2018a, Liu et al., 2018). The numerical resolution is ~4.5 km where the mesh node is within a 45-km distance from the nearest material interface (Fig. 10a), ~40 km where the node is >170 km away from the closest material interface, and linearly interpolated between 4.5 and 40 km at intermediate distances from material interfaces. The triangular mesh will be regenerated when the mesh is overly stretched, more details about this method can be found in Liu et al., 2018a, 2019b. and the Supplementary materials.

3.1. Possible origins of a buoyant Izanagi slab

According to previous numerical models, flat subduction of a buoyant oceanic plateau within an old oceanic plate beneath western North America (Liu et al., 2010) could have caused ~500–1000 m dynamic subsidence inside the overriding plate, e.g. may lead to widespread marine transgression (Fig. 4; Liu et al., 2008a). Therefore, the Yanshanian flat slab beneath East Asia, due to the lack of marine inundation, should be overall more buoyant compared to the Laramide slab. Possible mechanisms for reducing slab negative buoyancy may include 1) a subducting oceanic plateau and 2) subducting depleted mantle lithosphere.

In addition, the spatial range of crustal deformation and intraplate magmatism in East Asia affected by the Yanshanian flat subduction was enormous (1000 km E-W and >2000 km N-S) (Figs. 1, 3, 6–7), a candidate oceanic plateau that was proposed to cause the Yanshanian flat subduction (Wu et al., 2019) should also be very large, likely

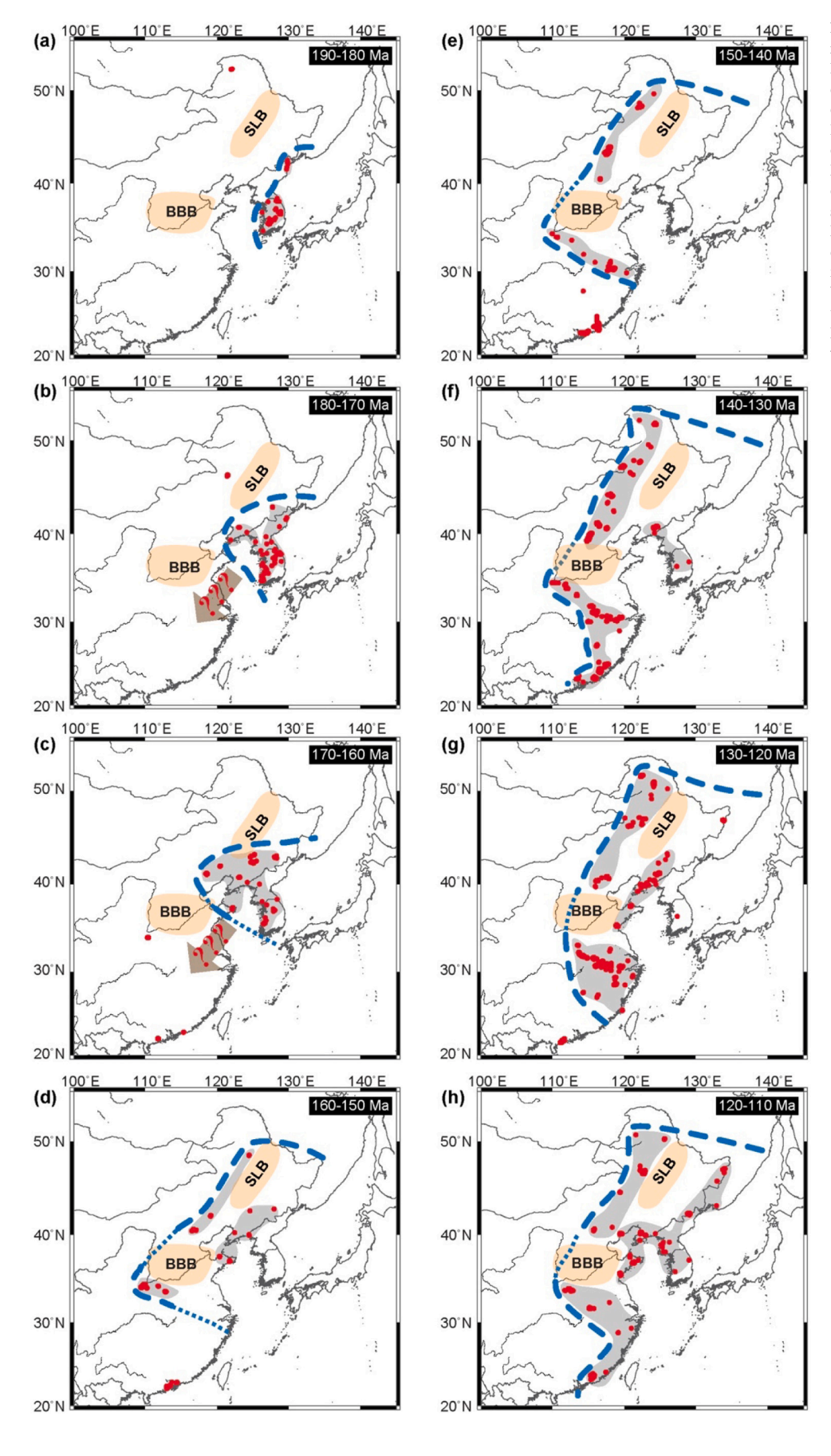


Fig. 6. Spatial and temporal distribution of magmatism in East Asia during ca. 190-110 Ma. (a-h) Distribution of magmatism (red dots) is represented in eight time periods. The data sources are the same as those in Fig. 3. Blue dashed contours mark the western edge of regions with active magmatism, and these lines are referred to as the magmatic front to conveniently represent the arc location and slab geometry when the amount of data is limited compared to that in Fig. 8. Blue dashed lines illustrate the deduced outlines for magmatism in regions that was covered by thick sediments or ocean. (For interpretation of the references to colour in this figure legend, the reader is referred to the web version of this article.)

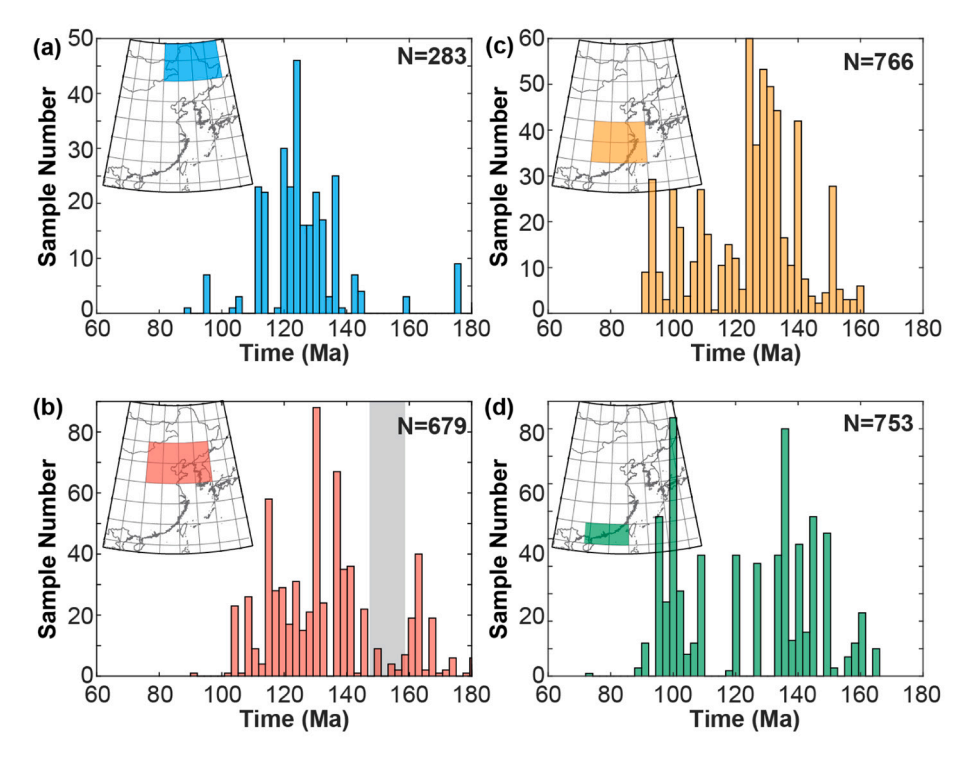


Fig. 7. Temporal distribution of igneous rocks in East Asia (from Wu et al., 2007; Niu et al., 2015; Kim et al., 2015; Yokoyama et al., 2016; Zhai et al., 2016). (a-d) Number density of igneous rocks as a function of age (data sources are the same as those in Fig. 3). The spatial division is also the same as that in Fig. 3. The grey shading in Panel b marks the brief attenuating period for intraplate magmatism (or magmatic gap).

broader than the proposed conjugate Shatsky Rise plateau that led to the Laramide deformation (Liu et al., 2010). Consequently, the candidate plateau for the Yanshanian tectonism could be physiographically similar to the Ontong Java Plateau (\sim 2000 km long and >1000 km wide). Lithospheric properties of the Ontong Java Plateau include: 1) the Moho is found to be \sim 25–40 km deep, and the Lithosphere-Asthenosphere Boundary (LAB) appears to be >120 km deep (Neal et al., 1997;Tharimena et al., 2016;Tonegawa et al., 2019); 2) the thick crust of the oceanic plateau implies the degree of mantle melting to be 17–31%, which would result in a \sim 85 km thick harzburgite-rich depleted mantle lithosphere (Neal et al., 1997).

Although the petrological and geochemical properties can be different, the geodynamic consequences of such a large oceanic plateau upon subduction could be similar to those due to subduction of a large piece of continental lithosphere such as the Indian subcontinent. A natural question is: how could such a buoyancy anomaly be subducted? Indeed, the Ontong Java plateau refused to enter the deep mantle due to its large buoyancy, which instead has shut down subduction in the southwest Pacific. However, if part of the low-density plateau crust was removed at the trench to accreted onto the upper plate, such as that implied for the oceanic plateaus along the west coast of North America (Tarduno et al., 1985; Liu et al., 2010), the reduced buoyancy may allow the plateau to eventually subduct. Furthermore, the Ontong Java Plateau was jammed at an ocean-ocean trench where the density contrast across the plate boundary is not as large as that for an oceancontinent interface that was the case during the Yanshanian flat slab. The same reasoning could apply to the subduction of continental lithosphere, where mechanical decoupling of the upper crust from the downgoing plate could allow subduction to continue (Capitanio et al., 2011; Ingalls et al., 2016).

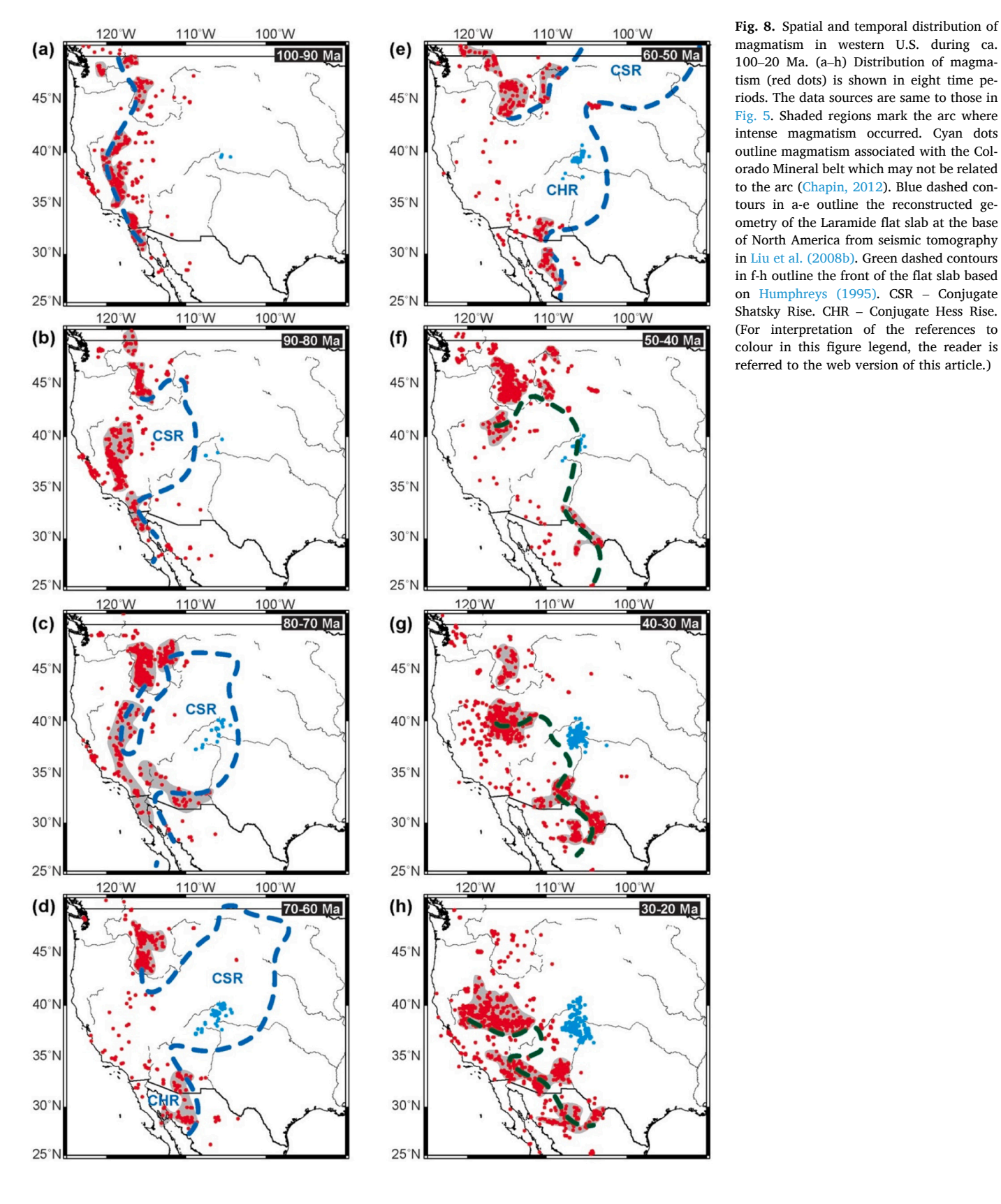
3.2. Key relevant geodynamic quantities

3.2.1. Setup of a generalized model

In order to construct a geodynamic model that could represent both

scenarios for an overall buoyant slab as discussed in the previous section, we will use the term "terrane" to interchangeably describe the oceanic plateau and the continental lithosphere that may have induced the Yanshanian flat subduction. According to the recent paleogeographic reconstruction (Liu et al., 2017;Li et al., 2019), this terrane could have been embedded within the Izanagi Plate during the early Mesozoic, with passive margins connecting to the surrounding seafloors (Fig. 1a). We assume an 80 Myr-old seafloor age for the Izanagi plate that carried the incoming terrane. The Izanagi Plate subducted below Eurasia at a trench-normal speed of ~5 cm/yr during the Jurassic, as is adopted as the kinematic boundary condition of the model (Fig. 10a). The imposed side velocity boundary condition represents the fact that the terrane motion is subject to that of the much-broader Izanagi Plate. According to the supplementary sensitivity tests, the specific convergence rate during flat subduction does not obviously affect the pattern of flat subduction (Fig. S2; Movies 1-4). See Supplements for more details of physical parameters.

For most of the models, we assume a 35-km thick crust and 80-km thick depleted mantle for the terrane lithosphere, similar to the configuration of a large oceanic plateau like Ontong Java or a large piece of continental lithosphere. The width of the terrane is assumed to be 800 km (Fig. 10a). In the supplementary sensitivity tests, both the density and the width of the terrane are chosen to be free parameters. Through testing these parameters, we find that a small and/or dense terrane cannot sustain a wide flat subduction (Figs. S3-S4). In the reference model, the overriding plate is set to be 100 km thick close to the trench, increasing to 200 km thick into the continental interior (Fig. 10a). This simple set-up is based on the geological observations that 1) the Northeastern Asia is mainly composed of Phanerozoic terranes (Wu et al., 2011), and 2) when the flat slab migrated to a region beneath the Eastern North China Craton (ca. 150-140 Ma, Fig. 2c), the cratonic lithosphere could have been partially thinned, evidenced in the widespread magmatism by then (Figs. 6-7) (Yang et al., 2008; Meng et al., 2020; Xu. 2001; Liu et al., 2019a). With more sensitive tests (Fig. S5), we find that the thickness of the overriding plate does not obviously affect



magmatism in western U.S. during ca. 100-20 Ma. (a-h) Distribution of magmatism (red dots) is shown in eight time periods. The data sources are same to those in Fig. 5. Shaded regions mark the arc where intense magmatism occurred. Cyan dots outline magmatism associated with the Colorado Mineral belt which may not be related to the arc (Chapin, 2012). Blue dashed contours in a-e outline the reconstructed geometry of the Laramide flat slab at the base of North America from seismic tomography in Liu et al. (2008b). Green dashed contours in f-h outline the front of the flat slab based on Humphreys (1995). CSR - Conjugate Shatsky Rise. CHR - Conjugate Hess Rise. (For interpretation of the references to colour in this figure legend, the reader is referred to the web version of this article.)

the evolution of flat subduction, especially if its mantle lithosphere was weakened by some preceding modifications (Niu, 2005; Zhang et al., 2008; Wu et al., 2019; Hong et al., 2020; Zheng et al., 2018; Zhu and Xu, 2019).

3.2.2. Key rheological parameters

Following the previous studies, during the subduction process, the terrane crust is assumed to have a yielding stress of 200 MPa, with a 15km thick weak middle crust (Fig. 10b) (Ranalli and Murphy, 1987;

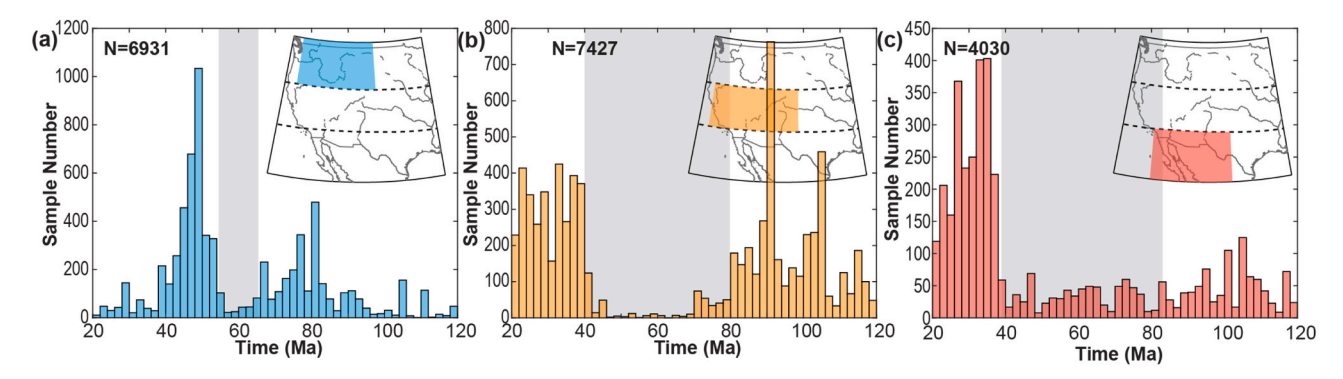


Fig. 9. Temporal distribution of igneous rocks in western N. America. (a–c) Number density of igneous rocks as a function of age (data sources are same as those in Fig. 5). The spatial division is the same as that in Fig. 5. The grey shading marks the attenuating period for intraplate magmatism (magmatic lull or gap).

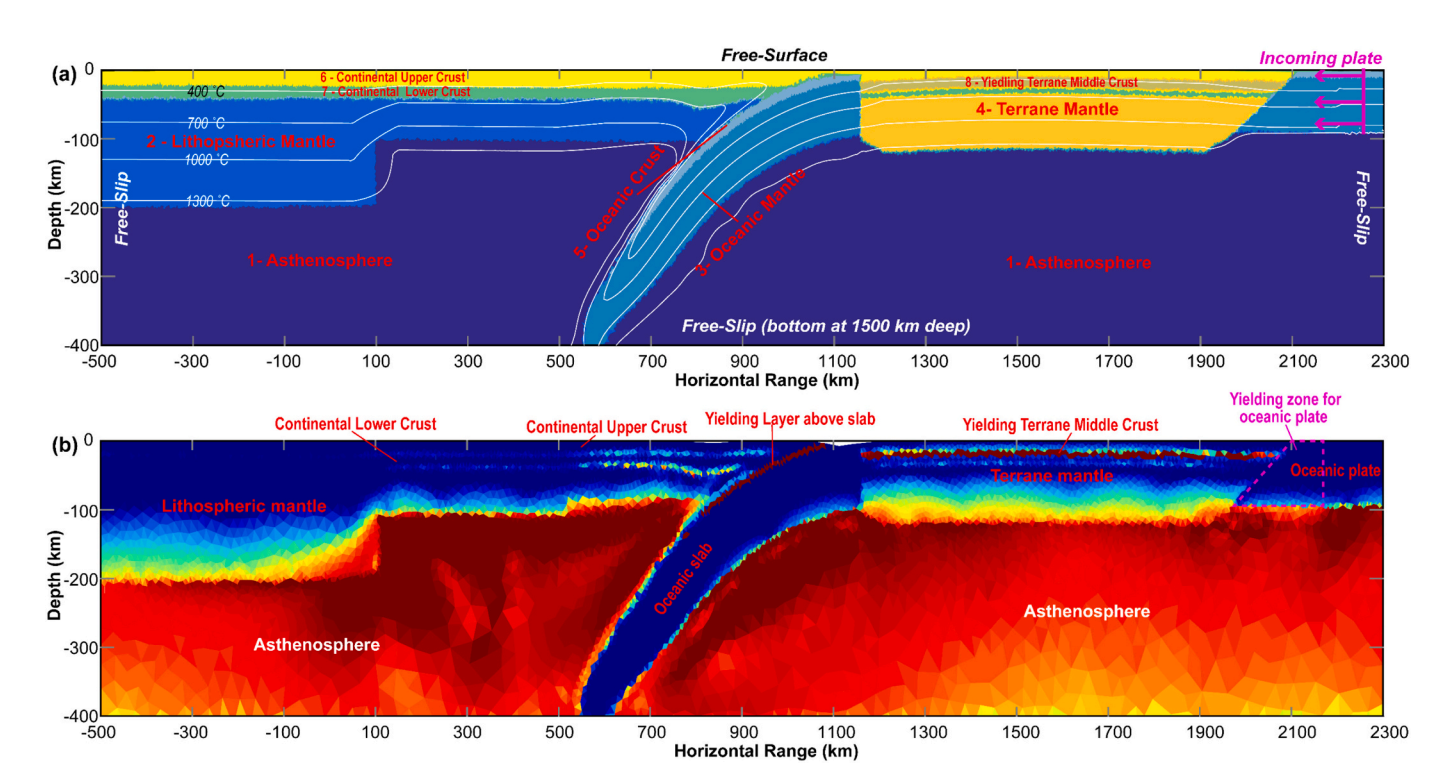


Fig. 10. Set-ups of the numerical models. (a) The 2D numerical box is 2800 km wide \times 1500 km deep. A free surface boundary condition is used at the top, and a free-slip condition is used for other boundaries. The horizontal velocity for the incoming plate is added between 2200 and 2250 km and above 90 km depth (cf. Gerya and Meilick, 2011). The surface temperature is fixed to be 0 °C and the bottom temperature is set to be the potential temperature of ambient mantle at 1350 °C. The continental portion includes a 20-km-thick upper crust, 20-km-thick lower crust, and 60-km-thick subcontinental mantle lithosphere close to the slab that increases to 140 km thick in the continental interior. The oceanic portion includes a 9-km-thick oceanic crust and 81-km-thick lithospheric mantle. The initial temperature profile of the continental or terrane portions follows a 1-D steady-state conductive thermal profile down to the bottom of lithosphere, and that of the oceanic plate follows a half-space cooling solution assuming an 80-Ma oceanic plate. White lines demonstrate the temperature contours. (b) The initial viscosity structure of the reference model. Note the plastic yielding of the plate interface and the terrane's middle crust. The oceanic plate following the terrane has not yielded yet due to the lack of deformation. Model parameters are in Table S1.

Tapponnier et al., 1990;Beaumont et al., 2006;Capitanio et al., 2011; Ingalls et al., 2016). The weak middle crust is assumed to be caused by the presence of water-enriched minerals like amphibole, and its strength can be further reduced when melting happens (Ranalli and Murphy, 1987;Tapponnier et al., 1990;Beaumont et al., 2006). This weak crustal layer will help to decouple the upper crust from the underlying lithospheric layers, thus allow most of the terrane mass to subduct, as discussed above.

Once the down-going plate reaches deeper than 200 km, dehydration starts that quickly forms a 10 km-thick weak (10^{19} Pa·s) layer along the plate interface between ca. 50 and 200 km depths (Fig. 10b) (Dobson

et al., 2002;Zhong and Li, 2020). The plates within 150 km distance from the passive margins is presumed to have a yielding stress of 200 MPa, which allows for strain accommodation and deformation within the subducting lithosphere (Fig. 10b) (Stern and Gerya, 2018). We assume that the overriding plate has a relative low yielding stress at 100 MPa during terrane subduction, considering the fact that mechanical deformation and melts/fluids infiltration would have previously weakened the upper plate (Figs. S2) (Niu, 2005;Zhang et al., 2008;Wu et al., 2019;Hong et al., 2020;Zheng et al., 2018;Zhu and Xu, 2019). The above yielding stresses are consistent with the inferred deviatoric stresses within present orogenic regions (Ghosh and Holt, 2012). Since the

model adopts an adaptively refined finite-element mesh with a real freesurface, the evolution of the topography caused by lithospheric deformation can be accurately calculated (Figs. 10–12).

3.2.3. Melting functions

Besides deformation, we also track the spatial and temporal evolution of melting, which is subsequently compared with the observed magmatic records (Figs. 3, 5, 6–9). We adopt a continental crustal solidus following previous experimental results (López and Castro, 2001; Liu et al., 2018a;Liu et al., 2018) and that for asthenospheric melting following the parameterization of Katz et al. (2003), all shown in Figure S6. In the sensitivity tests for crustal melting, the crustal solidus is perturbed to demonstrate its effect on melt formation and distribution (Fig. 13). Flux melting in the mantle wedge is presumed to occur at the location where subducted crust experiences dehydration, which occurs between 50 and 200 km depths and at temperatures higher than 700 °C (Dobson et al., 2002) (Fig. 12). Although more sophisticated melting functions are certainly possible, we prefer the relatively simple calculation adopted here, as we mostly focus on the first-order constraints on the composition and distribution of magmatism during terrane subduction and accretion. As a result, both the melt percolation process and its effects on rheology and temperature are not considered.

4. Intraplate tectonism during terrane subduction: A numerical perspective

Here we analyze the surface responses during a terrane-induced flat slab. Specifically, we focus on examining upper plate deformation, surface topography, and the resulting magmatic history, all of which have their observational counterparts (Figs. 1–3, 6 and 7). We also attempt to constrain the tectonic origin of the East Asian magmatism by analyzing the temporal-spatial patterns of modeled melts using different solidi.

4.1. The reference scenario

Figs. 11 and 12 demonstrate a typical model scenario for the advance and retreat of a flat slab beneath the overriding continent, whose associated surface responses closely resemble the late Mesozoic tectonism of East Asia. As the terrane approaches the trench, the convergence between the two plates are mainly accommodated by the terrane crust, leading to a decoupling zone along the weak middle crust and a weakened ocean-continent transition zone within the downgoing slab (Figs. 10, 11a, 12a and S7). When the buoyant terrane lithosphere (including part of the middle crust, the lower crust and the lithospheric mantle) enters the trench, the dense sinking oceanic slab (Table S1) at the front tears off and the back-arc region switches from extension to shortening, as seen from the topographic inversion of the back-arc

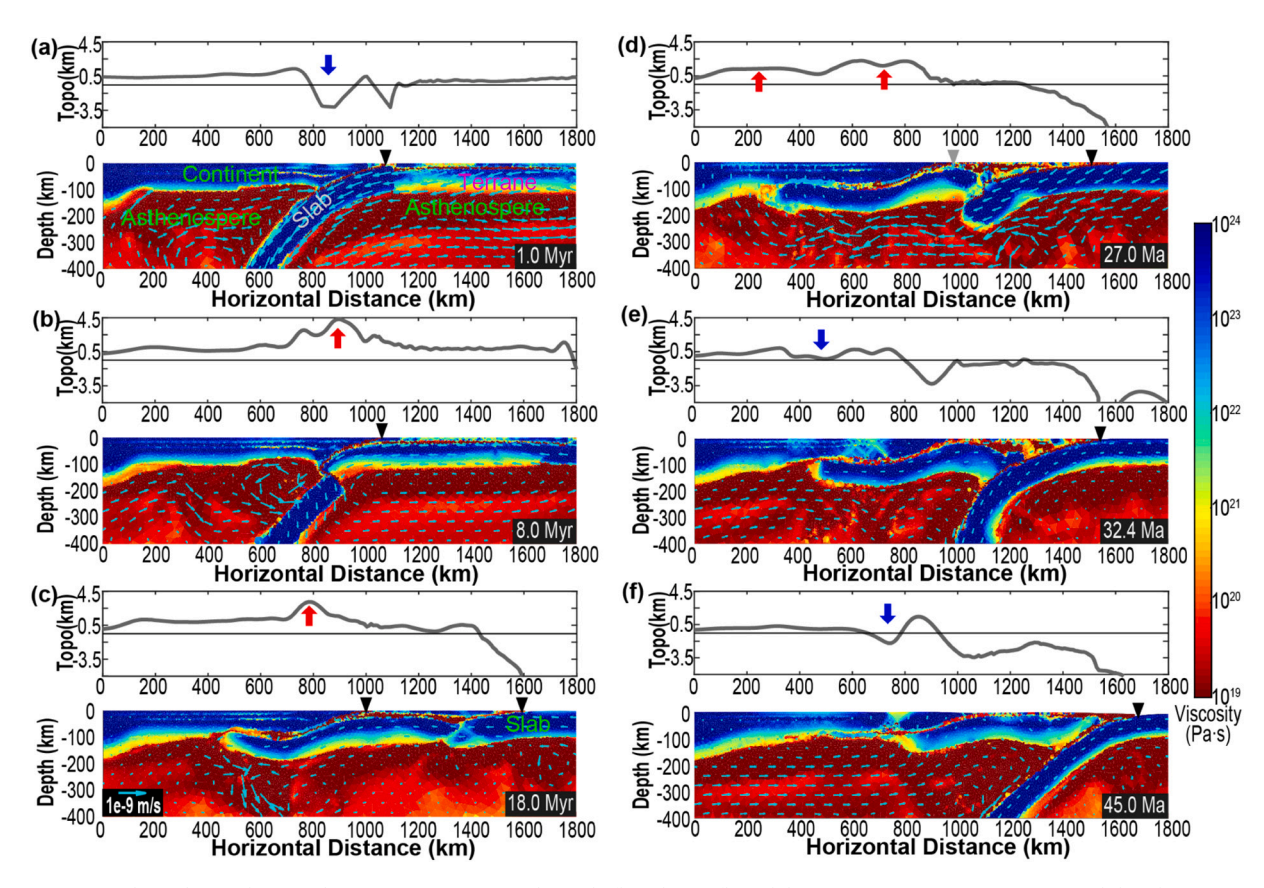


Fig. 11. 2D numerical simulation showing the viscosity structure and mantle flow during flat subduction. (a) An intra-oceanic terrane lithosphere moves with the surrounding oceanic lithosphere towards the trench. The black triangle marks the location of the active trench. The downward blue arrow marks the location of surface subsidence. Topo- Topography. (b) After the terrane enters the trench, the terrane lithosphere starts to underplate the overriding plate, forming low-angle subduction. This is accompanied by tearing off and sinking of the oceanic slab in front of the terrane. The upward red arrow marks the location of lithosphere shortening and surface uplift. (c) Inland migration of the flat slab causes more widespread upper plate uplift. (d) The flat terrane reaches a maximum inland distance, leading to a vast plateau topography. A new ocean-terrane subduction zone appears at the rear of the terrane. The grey triangle marks the abandoned trench after the trench jump. (e) Sinking of the new oceanic slab leads to terrane retreat, causing rifting of the overlying plate and asthenospheric upwelling in the wake of the retreating terrane. (f) Continuing retreat causes the locus of lithospheric extension, surface subsidence and upwelling asthenosphere to migrate towards the trench. (For interpretation of the references to colour in this figure legend, the reader is referred to the web version of this article.)

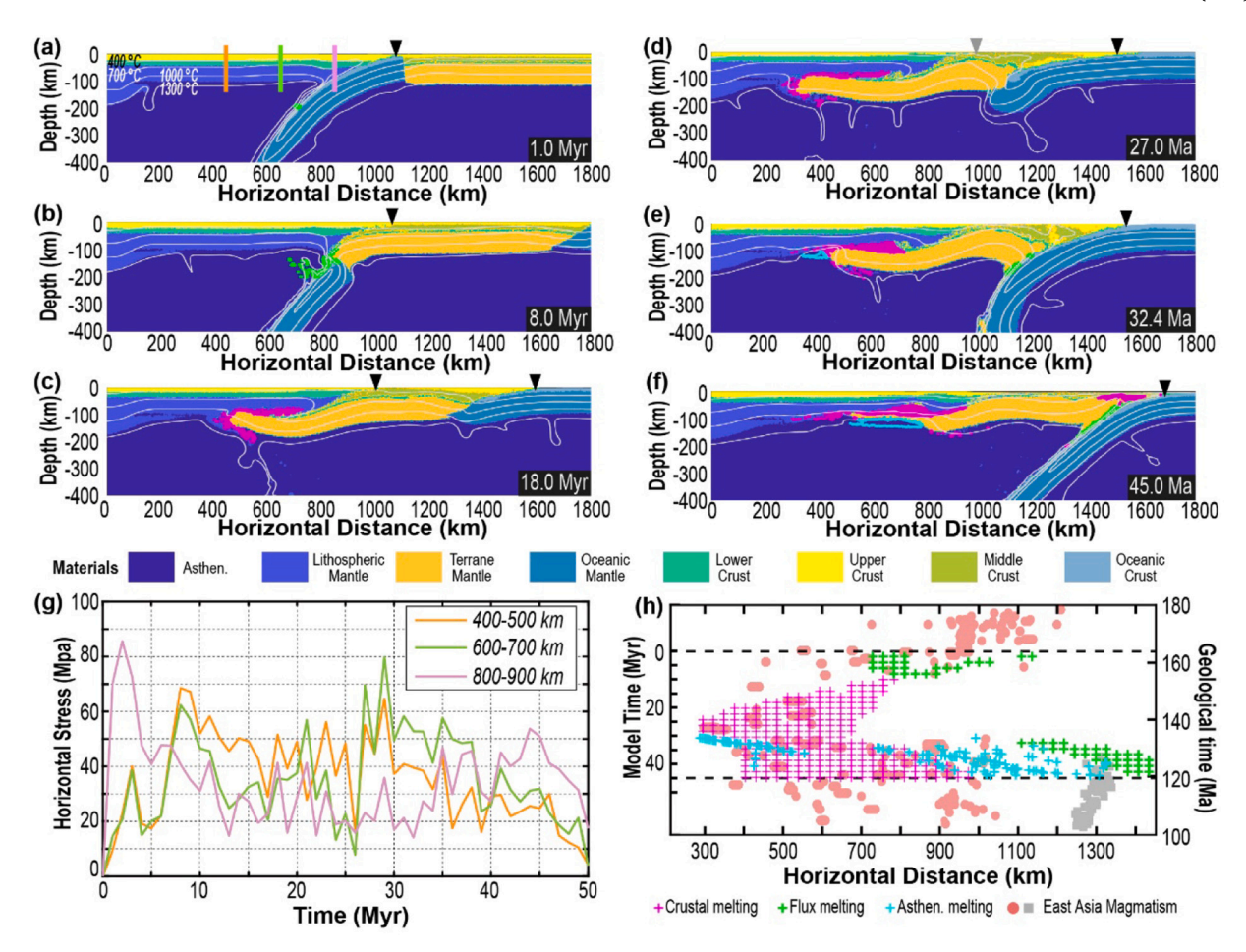


Fig. 12. Melting history of the terrane crust and the asthenosphere. (a-f) Same as Fig. 11 but shown with the composition field. During this process of flat subduction, the terrane mantle does not melt due to its high solidus (Fig. S6). After the initiation of the second subduction system, most of the terrane slab is pulled back to the east. Eventually, the terrane lithosphere moves away from the region with intense intraplate deformation. Temperature contours are in white. Light green contours in b, e and f mark the regions for dehydration of the subducted crust, implying flux melting in the above mantle wedge; purple contours in c-f illustrate regions for the melting of terrane crust (see Fig. S8 for the enlarged view of these contours). Light blue contours in e and f show regions for decompression-melting of upwelling asthenosphere. The black triangle marks location of active trenches. The grey triangle marks the abandoned trench after the trench jump. Asthen.- Asthenosphere. (g) Volume-averaged magnitudes of the horizontal stress as a function of time at three cross sections of the overriding plate, with locations shown as vertical colour columns in A. major stages of the subduction history can be recognized: (1) the break-off of the prior oceanic slab causes the abrupt increase of the horizontal stress between 0 and 5 Myr in the 800-900 km line. (2) propagation of the continental terrane leads to enhanced stress during 7 to 12 Myr along the 400-500 km and 600-700 km lines. (3) the second subduction phase causes widespread extension during 18 and 30 Myr along all lines. (h) Comparison between observed magmatism and predicted melting from the model. Observed magmatism is the same as that in Figs. 3 & 15. Considering ~30% E-W bulk extension occurred in North China after ca. 140 Ma (Liu et al., 2017), and the amount of trench-jump during magma retreat (Figs. 15a & b), we restore the paleo-position of the magmatic belt based on that in Fig. 15d. Modeled melting of the terrane crust (purple) and the mantle wedge (light green) is shown at every 25 km in the horizontal direction. Asthenospheric melting (light blue) is shown as locations where the fasted upwelling meets the melting condition, to illustrate the peak decompression melting. Two black dashed lines illustrate the time range of the numerical model. Magmatism earlier or later than the chosen model duration is not compared to model predictions. (For interpretation of the references to colour in this figure legend, the reader is referred to the web version of this article.)

(Fig. 11a vs. b; Fig. 12b). As previous studies showed (Liu and Currie, 2016), tearing and detachment of the proceeding dense slab can promote the formation of flat subduction. Accompanying this slab tearing event, the resulting localized uplifts (both near the trench and in the far interior) could explain the first regional unconformity at ca. 165 Ma in East Asia (Fig. 2). Contemporarily, small amounts of continental crust enter the subduction channel, forming a 'cold plume' (Li and Gerya, 2009) (Figs. 12b, S7). Presence of continental materials in the hydrated mantle wedge could significantly decrease melting temperature (Katz et al., 2003), causing subduction-related magmatism close to the Jurassic and Cretaceous trenches (Guo et al., 2015; Wu et al., 2011) (Fig. 3).

The terrane lithosphere keeps advancing to form a flat-lying slab, leading to a landward migration of both the high topography (Fig. 11b-d) and the peak horizontal lithospheric stress (Fig. 12g), where the resulting differential subsidence (reflected in both

topography and stress) can contribute to the locally preserved 165–140 Ma sedimentation in the continental interior (Li et al., 2019;Liu et al., 2017;Wu et al., 2019) (Fig. 1). As the flat slab approaches its maximum inland extent, the topographic gradients gradually diminish and eventually form a high-elevation plateau (Fig. 11c, d), during which the lithospheric stress also becomes more evenly distributed (Fig. 12g). This plateau or a later peneplain could correspond to the second unconformity at ca. 140 Ma (Fig. 2) (Li et al., 2019;Liu et al., 2017;Wu et al., 2019). During this stage of slab advance, the lower terrane crust at the tip of the advancing flat slab gets heated to above the melting point, and the resulting melt migrates inland with a rate roughly matching that observed in East Asia (Fig. 3 vs. 12 h; Fig. 12c, d). See supplementary Movies 1–4 for more details.

Due to both the push-back by the thicker lithosphere on the left and gravitational instability developed at the rear of the terrane, a new ocean-continent subduction zone ultimately forms (Fig. 11c, d; Fig. 12c,

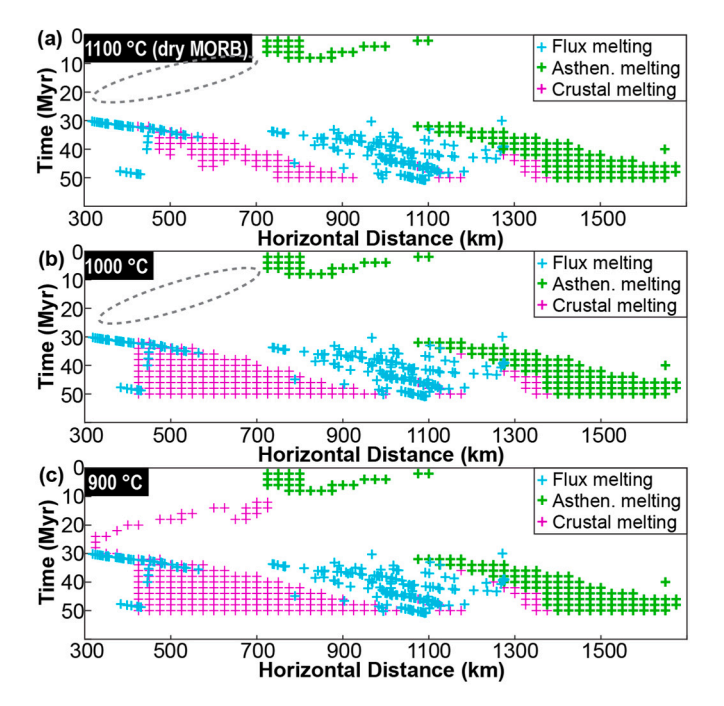


Fig. 13. Sensitivity test for crustal melting. (a-c) Same as Run 1, but with the crustal solidus increased by 300 °C, 200 °C, and 100 °C respectively. The temperature value in each panel corresponds the solidus of the terrane crust at \sim 40 km depth. The grey dashed ellipsoid in panel a and b illustrates a period for magmatic quiesce.

d). Sinking of the new oceanic slab into the upper mantle generates a fast (~7 cm/yr) retreat of the trench (Faccenna et al., 2017), which pulls the underplating flat slab towards the right (Fig. 11e; Fig. 12e). The effects of model parameters on terrane retreat are systematically evaluated in Fig S3-S5, S8. The retreating terrane lithosphere viscously stretches the overlying lithosphere from below and causes it to thin and rift (Figs. 12e; Fig. 12e). The region above the flat tip of the terrane rifts first, in response to the largest extensional stress (Fig. 11e; Fig. 12g). As the terrane translates eastward, the peak stress within the upper plate propagates towards the trench (Fig. 12g), so does surface subsidence (Fig. 11e, f); this corresponds to the observed eastward migrating crustal rifting in East Asia (Fig. 1b). Tests show that the extent of rifting also depends on the viscous coupling at the interface between the upper plate and retreating terrane, with a stronger coupling causing more rifting (Figs. 11, 12 vs. S8).

Retreating of the terrane lithosphere also excites asthenospheric upwelling and enhances mantle melting in the wake of the terrane (Fig. 11d-f; Fig. 12d-f), whose trench-ward migration also resembles that observed (Fig. 12h). Both the increasing melting extent and asthenospheric contribution during the retreating stage are consistent with the secular increase in the $\varepsilon Nd(t)$ of mafic magmas in North China (Xu, 2001; Zheng et al., 2018). The overriding mantle lithosphere could have been metasomatized during flat subduction and additional melts from this lithosphere would further enrich the composition of magmas (Niu, 2005; Wu et al., 2019; Zhang et al., 2008; Zheng and Dai, 2018; Zheng et al., 2018; Zhu and Xu, 2019; Hong et al., 2020). After the normal subduction re-establishes, dehydration of the subducted crust and accompanying flux melting also resume (Fig. 12e, f, h). Upper-plate extension could facilitate melt underplating beneath the Moho to raise crustal temperature, which can trigger melting of the overriding crust (Liu et al., 2018; Zhou and Li, 2000) and partially contributing to the late stage (ca. <140 Ma) subduction-related granitoids in regions above the new subduction zone, e.g. in Korea Peninsular and Northeast China (Figs. 3 & 15).

4.2. Sources of melting for East Asian intraplate magmatism

The reference model (Run 1) adopts an amphibolite-like solidus (~800 °C at 40 km deep) (Fig. S6) which allows the model to reproduce both the advance and retreat of the observed magmatic migration in East Asia (Fig. 3c). We note that this solidus appears to be too low compared to that of MORB-rich oceanic crust (>1100 °C) (cf. Pertermann and Hirschmann, 2003), the commonly assumed source of melting during oceanic flat subduction. Therefore, we re-calculated the instantaneous melting behavior in Run 1 by increasing the solidus of the terrane crust (Fig. 13). These different solidi respectively correspond to that of dry MORB (~1100 °C at 40 km deep, Fig. 13a) and two other scenarios with crustal composition varying between MORB and amphibolite (Fig. 13b–c). In nature, this variation of crustal solidus can be caused by the variable water content or water-rich minerals like amphibole (López and Castro, 2001;Katz et al., 2003;Zheng et al., 2018;Wu et al., 2019; Zhu and Xu. 2019).

Based on these results, we find that an MORB-like solidus for the terrane crust (Fig. 13a) can only reproduce the trench-ward migration of the magmatic arc. This behavior is observed in some region (between 35 and 25°N) of East Asia (Fig. 3d) and above the entire Laramide flat slab in western U.S. (Fig. 5b, c), where the observed magmatism corresponded to the detachment/retreating of the flat slab (Fig. 12). In contrast, the terrane crust that generated the North China magmas with both advancing and retreating migration (Fig. 3c) should have a melting temperature no higher than 900 °C at 40 km depth, which is significantly lower than that of a MORB-like crust. Together, this outlines a composite flat slab below East Asia whose composition varied from amphibolite-rich (resembling continental crust) on the north to MORB-rich (resembling oceanic crust) on the south.

5. Discussion

5.1. On the nature of the East Asian flat slab

With quantitative numerical simulations (Figs. 11–12), we show that the observed J2-K1 tectonism in East Asia can be readily explained as surface responses during flat-slab subduction (Zheng et al., 2018; Wu et al., 2019; Zhu and Xu, 2019). Furthermore, these numerical calculations allow more in-depth understanding on the nature of the flat slab and how the East Asian Yanshanian slab differs from the western U.S. Laramide slab (Fig. 14).

More specifically, formation of the Laramide flat slab in western U.S. was contemporaneous with widespread inland subsidence within westcentral North America (Figs. 4, 14a). This is commonly attributed to downward dynamic pull from a long segment of Farallon slab attached to the inland side of the flat slab (Fig. 14a; Liu et al., 2008a, 2011). Differently, the advancing Yanshanian flat slab in East Asia was accompanied with episodes of regional-scale basin inversion and uplift within the overriding plate (Figs. 1–2, 14b). The contrasting topographic expression in the latter case could be ultimately attributed to a more buoyant flat slab, which caused the previously attached oceanic slab on the west to break off and led to overall surface uplift (Figs. 11, 12). To this end, both the low-density Ontong-Java-type oceanic mantle lithosphere and the sub-continental mantle lithosphere might work. However, as discussed earlier, both cases need to have some crust removed in order for the lithosphere to subduct. Therefore, unless the large oceanic plateau has a weak internal layer to decouple part or most of its crust during subduction, the continental lithosphere whose crust is naturally weaker (Ranalli and Murphy, 1987; Beaumont et al., 2006) can represent a better candidate for the formation of the Yanshanian flat slab. Indeed, this statement of a continental flat slab is further supported by the accreted J2-K1 continental terrane crusts along the East Asian margin (Fig. 1a). In contrast, there are no large-scale oceanic crusts found to be accreted onto East Asia during the Mesozoic at the latitudes similar to North China and Northeast China.

L. Liu et al. Earth-Science Reviews 214 (2021) 103505

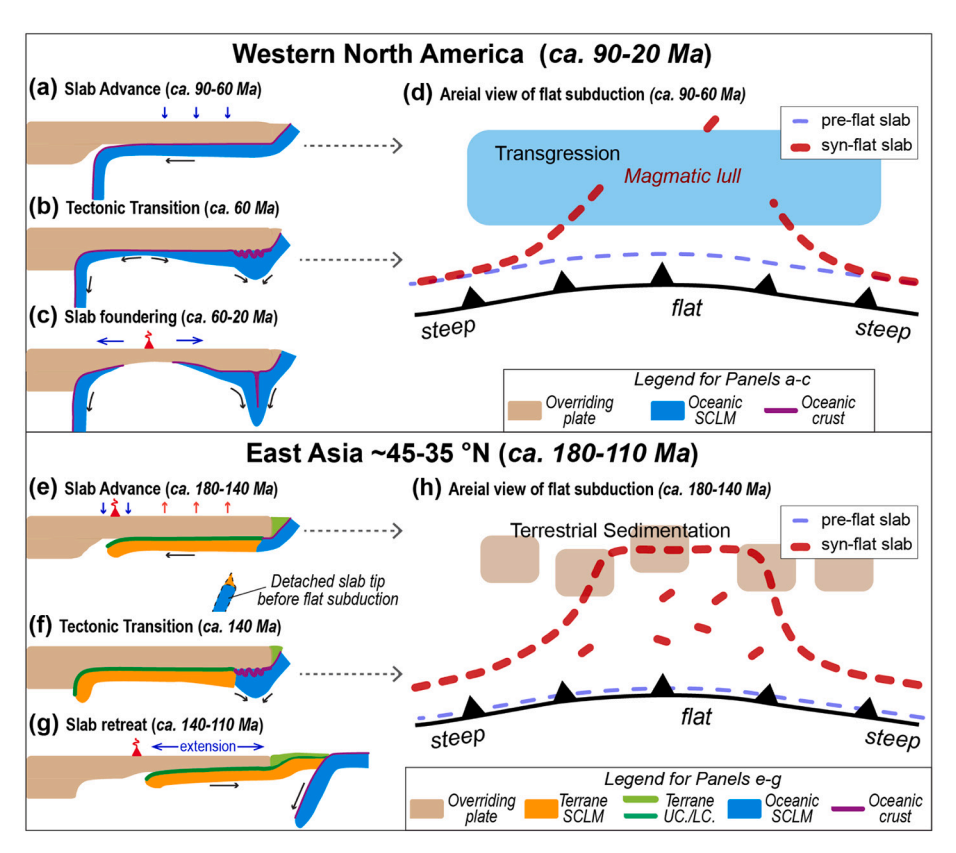


Fig. 14. Summary of the flat subduction beneath western US. and East Asia. (a) Beneath the western U. S., the landward motion of the flat slab mainly occurred during ca. 90-60 Ma. (b) At ca. 60 Ma, downward pulling from both the tip and rear side of the slab broke up the flat slab itself. (c) After ca. 60 Ma, the tip of flat slab sunk into the deep mantle, and the rear slab retreat towards the trench. This caused a magmatic flare-up in the overriding plate that also migrated towards the trench. (d) In the map view, widespread marine transgression happened in the overring plate as the magmatic arc migrated landward, eventually leading to a magmatic lull above the flat slab. (e) Beneath East Asia, slab advance happened during ca. 180 and 140 Ma. The low melting point of the terrane crust generated sustaining magmatism going with the slab. (f) Due to the increasing resistance from the overriding plate, deformation focused near the rear side of the terrane, causing a new subduction zone to form behind the flat slab. (g) During ca. 140–110 Ma, the newly subducted oceanic slab pulled the buoyant terrane slab backward. This process led to lithospheric rifting in the overriding plate. After the flat slab was removed. the bottom of the overriding plate (being volatile-rich already) contacted with the hot asthenosphere diachronously, experiencing both crustal and mantle melting. (h) In a map view, sedimentary basins experienced inversion during slab advance where locally preserved basins only recorded terrestrial sedimentation. In the meantime, the magmatic belt expanded landward, and magmatism remained mostly active throughout the region above the flat

Additional lines of evidence further reinforce the proposal that continental terrane subduction caused the Yanshanian flat slab. First, both landward and trench-ward migration of magmatism within North China (Fig. 3c) require a substantially lower solidus than that of a MORB-crust, thus favoring a continental flat slab (Figs. 12, 13). Second, as the flat slab moved inland, magmatism remained generally active above the slab (Figs. 6, 14b), with only a very brief <10 Myr magmatic gap as the slab reached its maximum extent (Fig. 7). This is in sharp contrast to the prominent magmatic lull commonly observed above an oceanic flat slab (Fig. 14d), including the Late-Cretaceous Laramide slab in western U.S. (Henderson et al., 1984;Liu, 2015), the late-Cenozoic Yakutat slab in southern Alaska (Finzel et al., 2011), and the ongoing Peruvian and Chilean flat slabs in South America (Gutscher et al., 1999). As shown in Fig. 13, if the slab crust has a MORB-like solidus, the magmatism in the overriding plate only develops a trench-ward migration during slab retreat, similar to that observed in western U.S. (Figs. 8, 9). Otherwise, with an amphibole-like solidus that is more common for continental lower crust (Fig. S6), both a prominent landward arc migration and sustaining supra-slab magmatism can result (Figs. 12h, 13c-d).

A potential counter argument to the above proposal is that petrologically, the crust of Yanshanian flat slab, even if oceanic in nature, could have been hydrated or metamorphosed to be water-enriched, and caused extensive melting beneath East Asia (López and Castro, 2001; Katz et al., 2003). However, based on the studies of magmatic geochemistry in North China where the landward migration of magmatism is the most apparent during flat subduction (Fig. 2c), direct contribution of oceanic compositions is generally missing, while the contribution from the in-suit ancient continental crust (e.g. crust of North and South China blocks) can be widely identified (Li et al., 2017; Menzies et al., 2007; Huang et al., 2012; Ma et al., 2012; Wu et al., 2005; Zhang et al., 2010a). This acts as another strong support to our proposal that the Yanshanian flat slab arose from subduction of continental

terranes, especially those with a paleogeographic affinity to the North China and/or South China blocks (Fig. 1).

5.2. The process of Mesozoic terrane accretion and subduction in East Asia

Inspired by the above analysis and the interpretation that the process of continental terrane accretion (Fig. 1a) led to a period of flat subduction beneath East Asia (Figs. 11, 12), we further performed a palinspastic reconstruction of the presently preserved terranes back to the Mesozoic. The preserved continental terranes along the East Asia margin are up to $\sim\!500$ km wide along the east-west direction and $\sim\!1200$ km long along the north-south direction (cf. Li et al., 2019). In an attempt to restore the configuration of these continental terranes back to the Mesozoic, we implemented a rather crude approach for palinspastic restoration (see the method in the supplements) (Figs. 1a & 15). Based on this reconstruction, we gained more insights on the mechanism of J2-K1 intraplate tectonism.

After the restoration of the terranes, the rearranged distribution of the Mesozoic magmas in East Asia becomes more continuous and more straightforward to interpret: the continental margins in Northeast China and South China recorded largely uninterrupted magmatism without obvious landward migration; the accreted terranes (e.g. Jiamusi and North Japan) only host magmatism younger than their accretion age, consistent with the geodynamic implication that terrane accretion occurred after a new subduction zone east of them was established (Figs. 3b, d, 15c, S1, 11–12).

The reconstruction may also help further explain some petrological properties of the intraplate magmatism. For example, the potential affinity of these terranes to the South China block (Isozaki et al., 2010; Kabir et al., 2018;Li et al., 2019) implies that during the flat slab stage, melting of the ancient continental crust that was carried down by the flat slab can readily explain the geochemical characteristics of the East Asian

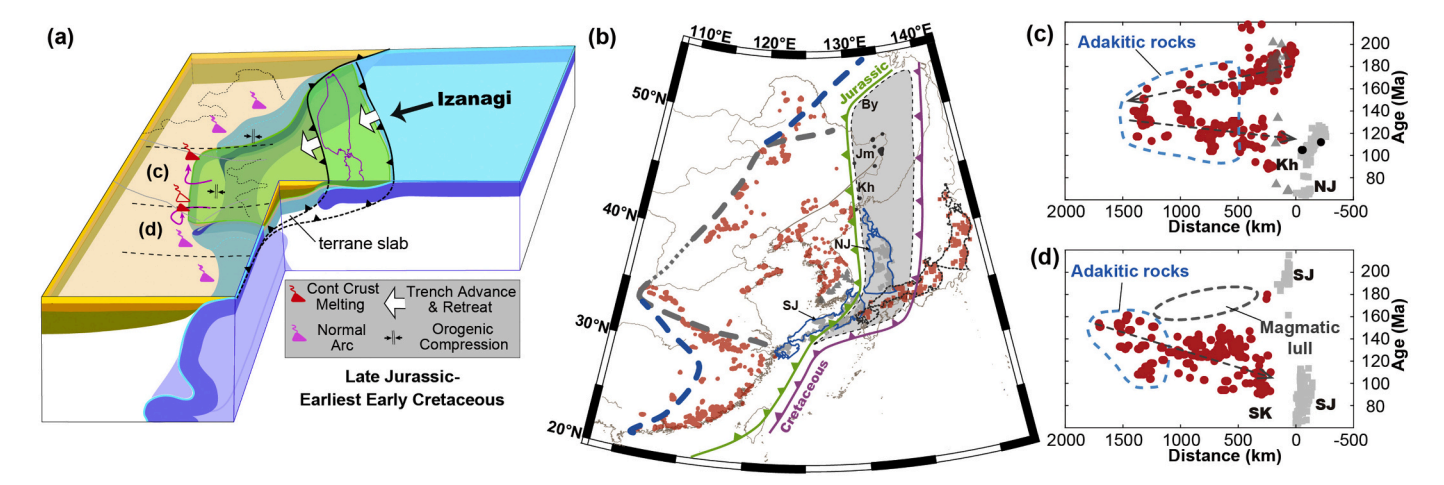


Fig. 15. Reconstructed Magma distribution of Late Mesozoic East Asia. (a) The accreted terrane lithosphere formed widespread flat subduction beneath Northeast Asia. (b) Map distribution of different types of magmas and the palinspastically restored Japanese islands, with the restoration based on the distribution of terranes, magmatism, metamorphic rocks and fossil tracks (Isozaki et al., 2010; Kabir et al., 2018; Khanchuk et al., 2016; Li et al., 2019; Liu et al., 2017; Matsukawa et al., 2005; Niu et al., 2015; Wu et al., 2011; Yokoyama et al., 2016; Zhou and Li, 2017) (see supplements). The grey shading with black dashed contour marks the potential range for the J2-K1 continental terrane(s). The green and magenta bold arrows mark subduction directions of the Izanagi Plate during Jurassic and Cretaceous, respectively (Liu et al., 2017). The grey dashed line outlines the plausible region mostly affected by the continental portion of the composite slab, while the blue dashed lines mark the possible inland extents of the oceanic portions of the composite slab. (c-d) Magma ages plotted against distance from the trench within 45°N- 35°N and 35°N- 25°N, respectively. Distance is calculated from the nearest Jurassic trench, with positive distance being west and negative east. The blue dashed contours in b and d mark the distribution of the adakitic rocks. Jm- Jiamusi terrane. Kh- Khanka terrane. By- Bureya terrane. NJ- North Japan. SJ- South Japan. (For interpretation of the references to colour in this figure legend, the reader is referred to the web version of this article.)

magmas (Menzies et al., 2007; Huang et al., 2012; Ma et al., 2012; Zhang et al., 2010a).

Finally, this palinspastic restoration, together with the upper plate tectonism clearly correlating with a single flat slab cycle, implies that a large contiguous continental terrane was subducted beneath and accreted onto East Asia in the Mesozoic. The notion that part of the terrane crust was subducted (Fig. 12) implies that the original terrane was likely larger in scale than that preserved now (Fig. 1). However, we emphasize that this restoration is restricted by data availability and quality, and that further evaluation with more abundant geological and paleomagnetic data is warranted.

5.3. Implications on terrane accretion

Some new insights may arise from our proposed model of terrane subduction and accretion. As demonstrated in the model (Figs. 11–12), a large amount of slab retreat happened after the formation of a new subduction zone behind the buoyant terrane lithosphere. On one hand, this process helps to explain 1) the trench-ward migration of magmatism, and 2) widespread crustal rifting and migration of depocenters (Figs. 1–3, 15). On the other hand, the implied post-accretionary extension could be accompanied by exhumation of both high-pressure (HP) metamorphic and ultra-high-pressure (UHP) metamorphic rocks.

However, the distribution of the UHP rocks is geographically variable. For example, UHP rocks are commonly found in central Qinling-Dabie Orogen (Wu and Zheng, 2013), but within the accretionary belts in East Asia they have been only reported in South Japan (Kabir et al., 2018). Here, the sparse distribution for the UHP rocks in East Asia is consistent with our models: although the deeply subducted terrane crust was gradually exhumated during the >20 Myr duration of terrane retreat, this crust was mostly buried by the upper crust, which was initially decoupled from the subducting slab and remained at the surface throughout the flat subduction cycle (Figs. 11–12, S7).

In reality, the exhumation character of subducted rocks is likely related to the mechanical property of the middle crustal layer of the slab. For example, a weak middle crust would decouple the upper crust from that underneath upon subduction (Beaumont et al., 2006;Tapponnier et al., 1990;Capitanio et al., 2011), while the accretion process would

mostly exhume terrane materials from the upper and middle crust (Figs. 11–12), which implies dominantly HP blue-schist and amphibolite close to the paleo-trenches (Kabir et al., 2018;Zhou and Li, 2017). In contrast, models without a weak middle crust would allow subduction of the upper crust, which helps to form buoyant upwelling and exhumation of UHP rocks (Li and Gerya, 2009).

Another outstanding question about continental accretion is that sometimes the amount of terrane convergence far exceeds that of the preserved crustal shortening (Cawood et al., 2009;Kapp and DeCelles, 2019). We suggest that this mismatch should partially reflect *syn*-convergence terrane subduction, during which much of terrane's lower crust enters the mantle, leaving the decoupled upper crust at the surface (Figs. 11–12, S7). In general, accretionary orogens around the world often record a lithospheric stretching stage following the main contractional period, likely as a result of terrane retreat during the establishment of a new subduction zone (Figs. 11–12). Notable examples include the Appalachian–Caledonian orogens and orogenic events associated with the closure of central-Asian and (paleo-)Tethyan oceans (Cawood et al., 2009;Meng, 2003; Kapp and DeCelles, 2019).

Finally, terrane accretion also seems to modulate the tempo and style of subduction by forming oceanward trench jumps (Figs. 11–12, S7). This appears to be a common process during the Phanerozoic assembly of circum-Tethyan terranes (Kapp and DeCelles, 2019; Wan et al., 2019), with a contemporary example being the formation of extensive reverse faults within the northern Indian ocean (Bull et al., 2010), implying a possible incipient intra-oceanic subduction zone.

5.4. The region of East Asia affected by terrane subduction

We note that the tectonic complexity of East Asia increased towards the Central Asia Orogenic Belt (CAOB, Fig. 1a) that was developed after the closure of paleo-Asian Ocean(s) (cf. Liu et al., 2017). Post-collisional evolution of the CAOB, e.g. via gravity collapse, has been proposed to influence the nearby Mesozoic sedimentation (e.g. Erlian and Songliao basins) and magmatism (Meng, 2003; Wang et al., 2015), in addition to the role of paleo-Pacific subduction as proposed here and in other studies (Li et al., 2019; Zheng and Dai, 2018; Zhu and Xu, 2019). It appears that two distinct Mesozoic tectonic domains coexisted in East Asia

that might have been controlled by subduction of the paleo-Asian and the paleo-Pacific plates, respectively.

In an attempt to distinguish these two tectonic domains, Zhu and Xu (2019) suggested to use Greater Xing'an-Yanshan-Yinshan Mountain ranges as a rough boundary. This division is further supported by the sedimentary, magmatic and structural evidence listed above (Figs. 1, 3, 6–7, 15). However, it would be probably reasonable to assume that regions close to this boundary were influenced by both mechanisms. Based on the above analysis, we tentatively use the thick grey dashed line in Fig. 15b to illustrate the plausible range that was affected by the process of terrane subduction and accretion. It is also possible that this broad continental slab helped to raise and flatten the oceanic slab on both the north and south sides, forming an even broader composite flat slab (Fig. 15). This notion is supported by the magmatic records in the region between 35 and 25°N, where the landward migration of magmatism during flat subduction is missing (Figs. 3d, 13–14).

5.5. Implication on destruction of North China Craton

Another important component of the late Mesozoic East Asian tectonism is the destruction of the North China Craton (NCC) (Menzies et al., 1993;Wu et al., 2019;Zhu and Xu, 2019). This dramatic tectonic event is characterized by apparent lithosphere thinning and rifting, with proposed mechanisms including thermo-mechanical erosion (Xu, 2001), shortening-induced gravitational instability (Gao et al., 2004), extension-triggered delamination of the lower lithosphere (Liu et al., 2018a;Liu et al., 2018), or lithospheric weakening caused by infiltration of melts/fluids into the overriding craton (Niu, 2005;Wu et al., 2019; Zhang et al., 2008;Zheng et al., 2018;Zheng and Dai, 2018). Given the complex Mesozoic geological records in North China (Figs. 1–2) (Wu et al., 2019;Zhu and Xu, 2019), these previous studies suggest that the NCC destruction could not have been due to one single mechanism.

According to our numerical models (Figs. 11-12, S5 and S8), the Yanshanian flat subduction could be an additional important factor for the NCC destruction. As shown in Figs. 11-12, S5 and S8, the advancing flat slab "bulldozed" the lower lithosphere of the overriding plate inland (a process similar to that in Chen et al., 2020), while slab retreat stretched the overriding plate to generate rifting —both processes can weaken and thin the overriding lithosphere. Furthermore, the flat subduction could have triggered additional processes to facilitate NCC destruction. For example, the advancing/retreating flat slab may cause local instability and delamination of the overriding mantle lithosphere or crust (Gao et al., 2004; Xu et al., 2008; Zhang et al., 2010a; Liu et al., 2018a). In addition, melts and/or fluids released from the flat slab can metasomatize or rehydrate the lower lithosphere of the NCC (Fig. 12). Therefore, after slab retreat, the modified lower lithosphere can be thermo-mechanically eroded through small-scale convection (Niu, 2005; Liu et al., 2018; Wu et al., 2019; Zhu and Xu, 2019; Zheng and Dai, 2018; Zheng et al., 2018).

As noted above, the exact processes for the lithospheric thinning of the NCC still remain elusive (Menzies et al., 2007;Yang et al., 2008;Wu et al., 2008;Xu et al., 2009;Zheng et al., 2018;Liu et al., 2019a;Meng et al., 2020). For simplicity, in most of our simulations, the overriding plate is set to be uniformly thick. The reference model adopts a thin lithosphere in the eastern NCC assuming this part was already thinned before it was underlain by the flat slab (e.g. 150–140 Ma). Supplementary sensitivity tests further demonstrate that the thickness of the overriding plate does not obviously affect the overall evolution of the flat subduction (Fig. S5). In this paper, we primarily focus on the Yanshanian magmatism and crustal deformation within East Asia, a region larger than the eastern NCC, so a detailed discussion on the NCC destruction is out of the scope.

6. Conclusions

By comparing the corresponding geological records in East Asia and

western U.S., we found that the majority portion of the flat slab beneath East Asia seems to be caused by the subducting continental lithosphere during terrane accretion. This buoyant flat slab had likely carried a limited portion of the oceanic plate on the south to go flatly under South China. This composite flat-slab model could explain multiple unique tectonic characteristics within East Asia (Fig. 15a).

- 1) The Yanshanian flat slab beneath East Asia was more buoyant than that of the Laramide slab beneath western N. America. This resulted in mostly uplift instead of subsidence within the overriding plate during slab advance (Fig. 14). Due to its buoyancy, the flat slab would stay mostly below the base of the overriding plate instead of finally sinking into the deep mantle as an oceanic slab would do.
- 2) The solidus of the Yanshanian flat slab can be >300 °C lower than that of an oceanic crust. Consequently, the hot tip and edge of the flat slab can readily experience melting, and the locus of the induced magmatism in the overriding plate migrated with the advancing/retreating motions of the slab. This contrasts with the pronounced magmatic lull associated with an oceanic flat slab, as seen in western U.S.
- 3) The advancing and retreating motions of the flat slab caused respective upper-plate compression and extension. Both led to thinning and reworking of the overriding plate. The surface responded by forming migrating depocenters of sedimentary basins.
- 4) The small density, low solidus of melting, and the spatial-temporal correlation of the flat slab with terrane accretion support the notion that the Yanshanian flat slab should mostly consist of continental lithosphere. Subduction of this continental slab could have caused local flattening of the oceanic slab further south. We propose that this composite flat slab may have played an important role in the J2-K1 tectonism in East Asia, especially in regions away from the Central Asian Orogenic Belt.

Supplementary data to this article can be found online at https://doi.org/10.1016/j.earscirev.2021.103505.

Author contributions

L. Liu performed all numerical simulations and data analysis. L.J. Liu conceived the scientific idea and oversaw the project. Y.G. Xu initiated the collaboration and advised on tectonics and geochemistry. All authors participated in manuscript preparation.

Data and code availabilities

The datasets for Figs. 1, 3 and 5–9 are available from the cited papers and website. All figures and movies are produced by the equations in the appendixes, together with initial/boundary conditions and model parameters given in the manuscript. The source code can be provided upon request.

CRediT authorship contribution statement

Liang Liu: Data Curation, Methodology, Software, Investigation, Visualization, Formal analysis, Writing- Original Draft. Lijun Liu: Conceptualization, Data Curation, Methodology, Investigation, Visualization, Formal analysis, Writing- Review & Editing, Supervision, Project Administration, Funding acquisition. Yi-Gang Xu: Data Curation, Methodology, Visualization, Formal analysis, Writing- Review & Editing, Supervision, Project Administration, Funding acquisition.

Declaration of Competing Interest

The authors declare that they have no known competing financial interests or personal relationships that could have appeared to influence the work reported in this paper.

Acknowledgement

We thank Qiang Ma for helpful discussions on the geology of East Asia. L. Liu's stay at UIUC is jointly supported by UIUC and the Guangdong Provincial Post-doc Program. L.J. Liu acknowledges National Science Foundation grants EAR 1554554, 1565640, and the GeoThrust Foundation at UIUC. This research is also supported by National Natural Science Foundation of China (41688103), the National Program on Global Change and Air-Sea Interaction (GASI-GEOGE-02) and the Chinese Academy of Sciences (XDB18000000). We thank two anonymous reviewers for their constructive comments on an early version of this paper. We also thank Professor Douwe van Hinsbergen for his editorial effort.

References

- Andrés-Martínez, M., Morgan, J.P., Pérez-Gussinyé, M., Rüpke, L., 2015. A new freesurface stabilization algorithm for geodynamical modelling: Theory and numerical tests. Phys. Earth Planet. Inter. 246, 41–51.
- Beaumont, C., Nguyen, M.H., Jamieson, R.A., Ellis, S., 2006. Crustal flow modes in large hot orogens. Geol. Soc. Lond., Spec. Publ. 268 (1), 91–145.
- Bull, J.M., DeMets, C., Krishna, K.S., Sanderson, D.J., Merkouriev, S., 2010. Reconciling plate kinematic and seismic estimates of lithospheric convergence in the Central Indian Ocean. Geology 38 (4), 307–310.
- Capitanio, F.A., Faccenna, C., Zlotnik, S., Stegman, D.R., 2011. Subduction dynamics and the origin of Andean orogeny and the Bolivian orocline. Nature 480 (7375), 83–86. Cawood, P.A., Kröner, A., Collins, W.J., Kusky, T.M., Mooney, W.D., Windley, B.F., 2009.
- Cawood, P.A., Kroner, A., Collins, W.J., Kusky, I.M., Mooney, W.D., Windley, B.F., 2009. Accretionary orogens through Earth history. Geol. Soc. Lond., Spec. Publ. 318 (1), 1–36.
- Chang, C., Liu, L., 2019. Distinct responses of intraplate sedimentation to different subsidence mechanisms: Insights from forward landscape evolution simulations. J. Geophys. Res. Earth Surf. 124 (5), 1139–1159.
- Chang, C., Liu, L., 2020. Investigating the Formation of the Cretaceous Western Interior Seaway Using Landscape Evolution Simulations. GSA Bulletin.
- Chapin, C.E., 2012. Origin of the Colorado mineral belt. Geosphere 8 (1), 28-43.
- Chen, M., Shen, X., Leng, W., Chen, L., 2020. Destruction of Cratonic Lithosphere Induced by Oceanic Subduction Initiation. Geophys. Res. Lett. 47 (15), e2020GL089140.
- Coney, P.J., Reynolds, S.J., 1977. Cordilleran benioff zones. Nature 270 (5636), 403–406.
- Dabrowski, M., Krotkiewski, M., Schmid, D.W., 2008. MILAMIN: MATLAB-based finite element method solver for large problems. Geochem. Geophys. Geosyst. 9 (4).
- Davis, G.A., Darby, B.J., 2010. Early cretaceous overprinting of the Mesozoic Daqing Shan fold-and-thrust belt by the Hohhot metamorphic core complex, Inner Mongolia, China. Geosci. Front. 1 (1), 1–20.
- Davis, G.A., Cong, W., Yadong, Z., Jinjiang, Z., Changhou, Z., Gehrels, G.E., 1998. The enigmatic Yinshan fold-and-thrust belt of northern China: New views on its intraplate contractional styles. Geology 26 (1), 43–46.
- DeCelles, P.G., 2004. Late Jurassic to Eocene evolution of the Cordilleran thrust belt and foreland basin system, western USA. Am. J. Sci. 304 (2), 105–168.
- Dobson, D.P., Meredith, P.G., Boon, S.A., 2002. Simulation of subduction zone seismicity by dehydration of serpentine. Science 298 (5597), 1407–1410.
- Dong, S., Zhang, Y., Li, H., Shi, W., Xue, H., Li, J., Huang, S., Wang, Y., 2018. The Yanshan orogeny and late Mesozoic multi-plate convergence in East Asia—Commemorating 90th years of the "Yanshan Orogeny". Sci. China Earth Sci. 61, 1888–1909. https://doi.org/10.1007/s11430-017-9297-y.
- Faccenna, C., Oncken, O., Holt, A.F., Becker, T.W., 2017. Initiation of the Andean orogeny by lower mantle subduction. Earth Planet. Sci. Lett. 463, 189–201.
- Finzel, E.S., Trop, J.M., Ridgway, K.D., Enkelmann, E., 2011. Upper plate proxies for flatslab subduction processes in southern Alaska. Earth Planet. Sci. Lett. 303, 348–360.
- Gao, S., Zhang, B.R., Gu, X.M., Xie, Q.L., Gao, C.L., Guo, X.M., 1995. Silurian-Devonian provenance changes of South Qinling basins: implications for accretion of the Yangtze (South China) to the North China cratons. Tectonophysics 250 (1–3), 183–197.
- Gao, S., Rudnick, R.L., Yuan, H.L., Liu, X.M., Liu, Y.S., Xu, W.L., Ling, W.L., Ayers, J., Wang, X.C., Wang, Q.H., 2004. Recycling lower continental crust in the North China craton. Nature 432 (7019), 892–897.
- Gerya, Taras V., Meilick, F.I., 2011. Geodynamic regimes of subduction under an active margin: effects of rheological weakening by fluids and melts. J. Metamorph. Geol. 29 (1), 7–31.
- Ghosh, A., Holt, W.E., 2012. Plate motions and stresses from global dynamic models. Science 335 (6070), 838–843.
- Guo, F., Li, H., Fan, W., Li, J., Zhao, L., Huang, M., Xu, W., 2015. Early Jurassic subduction of the Paleo-Pacific Ocean in NE China: Petrologic and geochemical evidence from the Tumen mafic intrusive complex. Lithos 224, 46–60.
- Gutscher, M.-A., Olivet, J.-L., Aslanian, D., Eissen, J.-P., Maury, R., 1999. The "lost Inca Plateau": cause of flat subduction beneath Peru? Earth Planet. Sci. Lett. 171, 335–341.
- Heller, P.L., Liu, L., 2016. Dynamic topography and vertical motion of the US Rocky Mountain region prior to and during the Laramide orogeny. Bulletin 128 (5–6), 973–988.

- Henderson, L.J., Gordon, R.G., Engebretson, D.C., 1984. Mesozoic aseismic ridges on the Farallon plate and southward migration of shallow subduction during the Laramide orogeny. Tectonics 3 (2), 121–132.
- Hong, L., Xu, Y., Zhang, L., Liu, Z., Xia, X., Kuang, Y., 2020. Oxidized late Mesozoic subcontinental lithospheric mantle beneath the eastern North China Craton: A clue to understanding cratonic destruction. Gondwana Res. 81, 230–239.
- Hu, J., Liu, L., Hermosillo, A., Zhou, Q., 2016. Simulation of late Cenozoic South American flat-slab subduction using geodynamic models with data assimilation. Earth Planet. Sci. Lett. 438, 1–13.
- Hu, J., Liu, L., 2016. Abnormal seismological and magmatic processes controlled by the tearing South American flat slabs. Earth Planet. Sci. Lett. 450, 40–51.
- Huang, D.Y., 2015. Yanliao Biota and Yanshan Movement (in Chinese). Acta Palaeontol. Sin. 54, 501–546.
- Huang, X.L., Zhong, J.W., Xu, Y.G., 2012. Two tales of the continental lithospheric mantle prior to the destruction of the North China Craton: Insights from early cretaceous mafic intrusions in western Shandong, East China. Geochim. Cosmochim. Acta 96, 193–214.
- Humphreys, E.D., 1995. Post-Laramide removal of the Farallon slab, western United States. Geology 23 (11), 987–990.
- Ingalls, M., Rowley, D.B., Currie, B., Colman, A.S., 2016. Large-scale subduction of continental crust implied by India–Asia mass-balance calculation. Nat. Geosci. 9 (11), 848–853.
- Isozaki, Y., Aoki, K., Nakama, T., Yanai, S., 2010. New insight into a subduction-related orogen: A reappraisal of the geotectonic framework and evolution of the Japanese Islands. Gondwana Res. 18 (1), 82–105.
- Kabir, M.F., Takasu, A., Li, W., 2018. Metamorphic P-T evolution of the Gotsu blueschists from the Suo metamorphic belt in SW Japan: Implications for tectonic correlation with the Heilongjiang complex, NE China. Mineral. Petrol. 112 (6), 819-836.
- Kapp, P., DeCelles, P.G., 2019. Mesozoic–Cenozoic geological evolution of the Himalayan-Tibetan orogen and working tectonic hypotheses. Am. J. Sci. 319 (3), 159–254.
- Katz, R.F., Spiegelman, M., Langmuir, C.H., 2003. A new parameterization of hydrous mantle melting. Geochem. Geophys. Geosyst. 4 (9).
- Khanchuk, A.I., Kemkin, I.V., Kruk, N.N., 2016. The Sikhote-Alin orogenic belt, Russian South East: Terranes and the formation of continental lithosphere based on geological and isotopic data. J. Asian Earth Sci. 120, 117–138.
- Kim, S.W., Kwon, S., Ko, K., Yi, K., Cho, D.L., Kee, W.S., Kim, B.C., 2015. Geochronological and geochemical implications of Early to Middle Jurassic continental adaktic arc magmatism in the Korean Peninsula. Lithos 227, 225–240.
- Kusky, T.M., Windley, B.F., Wang, L., Wang, Z., Li, X., Zhu, P., 2014. Flat slab subduction, trench suction, and craton destruction: comparison of the North China, Wyoming, and Brazilian cratons. Tectonophysics 630, 208–221.
- Li, S., Wilde, S.A., He, Z., Jiang, X., Liu, R., Zhao, L., 2014. Triassic sedimentation and postaccretionary crustal evolution along the Solonker suture zone in Inner Mongolia, China. Tectonics 33 (6), 960–981.
- Li, S., Suo, Y., Li, X., Zhou, J., Santosh, M., Wang, P., Dai, L., 2019. Mesozoic tectonomagmatic response in the East Asian ocean-continent connection zone to subduction of the Paleo-Pacific Plate. Earth Sci. Rev. 192, 91–137.
- Li, S.G., Yang, W., Ke, S., Meng, X., Tian, H., Xu, L., He, Y., Huang, J., Wang, X.C., Xia, Q., Sun, W., 2017. Deep carbon cycles constrained by a large-scale mantle Mg isotope anomaly in eastern China. Natl. Sci. Rev. 4 (1), 111–120.
- Li, Z., Gerya, T.V., 2009. Polyphase formation and exhumation of high-to ultrahighpressure rocks in continental subduction zone: Numerical modeling and application to the Sulu ultrahigh-pressure terrane in eastern China. J. Geophys. Res. Solid Earth 114 (B9).
- Li, Z.X., 1994. Collision between the North and South China blocks: a crustal-detachment model for suturing in the region east of the Tanlu fault. Geology 22 (8), 739–742.
- Liu, J., Cai, R., Pearson, D.G., Scott, J.M., 2019a. Thinning and destruction of the lithospheric mantle root beneath the North China Craton: a review. Earth Sci. Rev. 196, 102873.
- Liu, J.L., Davis, G.A., Mo, J.I., Huimei, G.U.A.N., Xiangdong, B.A.I., 2008a. Crustal detachment and destruction of the keel of North China Craton: constraints from late Mesozoic extensional structures. Earth Sci. Front. 15 (3), 72–81.
- Liu, L., 2015. The ups and downs of North America: evaluating the role of mantle dynamic topography since the Mesozoic. Rev. Geophys. 53 (3), 1022–1049.
- Liu, S., Nummedal, D., Liu, L., 2011. Migration of dynamic subsidence across the Late Cretaceous United States Western Interior Basin in response to Farallon plate subduction. Geology 39 (6), 555–558.
- Liu, L., Spasojević, S., Gurnis, M., 2008b. Reconstructing Farallon plate subduction beneath North America back to the late cretaceous. Science 322 (5903), 934–938.
- Liu, L., Gurnis, M., Seton, M., Saleeby, J., Müller, R.D., Jackson, J.M., 2010. The role of oceanic plateau subduction in the Laramide orogeny. Nat. Geosci. 3 (5), 353–357.
- Liu, L., Morgan, J.P., Xu, Y., Menzies, M., 2018. Craton Destruction 2: Evolution of cratonic lithosphere after a rapid keel delamination event. J. Geophys. Res. Solid Earth 123 (11), 10–069.
- Liu, L., Morgan, J.P., Xu, Y., Menzies, M., 2018a. Craton destruction 1: Cratonic keel delamination along a weak midlithospheric discontinuity layer. J. Geophys. Res. Solid Earth 123 (11), 10–040.
- Liu, L., Liu, L., Xu, Y.G., Xia, B., Ma, Q., Menzies, M., 2019b. Development of a dense cratonic keel prior to the destruction of the North China Craton: Constraints from sedimentary records and numerical simulation. J. Geophys. Res. Solid Earth 124 (12), 13192–13206.
- Liu, S., Currie, C.A., 2016. Farallon plate dynamics prior to the Laramide orogeny: Numerical models of flat subduction. Tectonophysics 666, 33–47.

- Liu, S., Gurnis, M., Ma, P., Zhang, B., 2017. Reconstruction of northeast Asian deformation integrated with western Pacific plate subduction since 200 Ma. Earth Sci. Rev. 175, 114–142.
- López, S., Castro, A., 2001. Determination of the fluid-absent solidus and supersolidus phase relationships of MORB-derived amphibolites in the range 4–14 kbar. Am. Mineral. 86 (11–12), 1396–1403.
- Ma, Q., Zheng, J., Griffin, W.L., Zhang, M., Tang, H., Su, Y., Ping, X., 2012. Triassic "adakitic" rocks in an extensional setting (North China): melts from the cratonic lower crust. Lithos 149, 159–173.
- Ma, Q., Zheng, J.P., Xu, Y.G., Griffin, W.L., Zhang, R.S., 2015. Are continental "adakites" derived from thickened or foundered lower crust? Earth Planet. Sci. Lett. 419, 125–133
- Matsukawa, M., Shibata, K., Kukihara, R., Koarai, K., Lockley, M.G., 2005. Review of Japanese dinosaur track localities: implications for ichnotaxonomy, paleogeography and stratigraphic correlation. Ichnos 12 (3), 201–222.
- Meng, Q.R., 2003. What drove late Mesozoic extension of the northern China–Mongolia tract? Tectonophysics 369 (3–4), 155–174.
- Meng, Q.-R., 2017. Development of Sedimentary Basins in Eastern China during the Yanshanian Period. Bull. Mineral. Petrol. Geochem. 36 (4), 567–569.
- Meng, Q.R., Zhang, G.W., 1999. Timing of collision of the North and South China blocks: controversy and reconciliation. Geology 27 (2), 123–126.
- Meng, Q.R., Wu, G.L., Fan, L.G., Wei, H.H., 2019. Tectonic evolution of early Mesozoic sedimentary basins in the North China block. Earth Sci. Rev. 190, 416-438.
- Meng, Q.R., Wu, G.L., Fan, L.G., Wei, H.H., Wang, E., 2020. Late Triassic uplift, magmatism and extension of the northern North China block: Mantle signatures in the surface. Earth Planet. Sci. Lett. 547, 116451.
- Menzies, M., Xu, Y., Zhang, H., Fan, W., 2007. Integration of geology, geophysics and geochemistry: a key to understanding the North China Craton. Lithos 96 (1–2), 1–21.
- Menzies, M.A., Fan, W., Zhang, M., 1993. Palaeozoic and Cenozoic lithoprobes and the loss of >120 km of Archaean lithosphere, Sino-Korean craton, China. Geol. Soc. Lond., Spec. Publ. 76 (1), 71–81.
- Müller, R.D., Seton, M., Zahirovic, S., Williams, S.E., Matthews, K.J., Wright, N.M., Shephard, G.E., Maloney, K.T., Barnett-Moore, N., Hosseinpour, M., Bower, D.J., 2016. Ocean basin evolution and global-scale plate reorganization events since Pangea breakup. Annu. Rev. Earth Planet. Sci. 44, 107–138.
- Müller, R.D., Zahirovic, S., Williams, S.E., Cannon, J., Seton, M., Bower, D.J., Tetley, M. G., Heine, C., Le Breton, E., Liu, S., Russell, S.H., 2019. A global plate model including lithospheric deformation along major rifts and orogens since the Triassic. Tectonics 38 (6), 1884–1907.
- Neal, C.R., Mahoney, J.J., Kroenke, L.W., Duncan, R.A., Petterson, M.G., 1997. The Ontong Java Plateau. Geophys. Monograph Am. Geophys. Union 100, 183–216.
- Niu, Y., Liu, Y., Xue, Q., Shao, F., Chen, S., Duan, M., Guo, P., Gong, H., Hu, Y., Hu, Z., Kong, J., 2015. Exotic origin of the Chinese continental shelf: new insights into the tectonic evolution of the western Pacific and eastern China since the Mesozoic. Sci. Bull. 60 (18), 1598–1616.
- Niu, Y.L., 2005. Generation and evolution of basaltic magmas: some basic concepts and a new view on the origin of Mesozoic–Cenozoic basaltic volcanism in eastern China. Geol. J. China Univ. 11 (1), 9–46.
- Pertermann, M., Hirschmann, M.M., 2003. Partial melting experiments on a MORB-like pyroxenite between 2 and 3 GPa: Constraints on the presence of pyroxenite in basalt source regions from solidus location and melting rate. J. Geophys. Res. Solid Earth 108 (B2).
- Ranalli, G., Murphy, D.C., 1987. Rheological stratification of the lithosphere. Tectonophysics 132 (4), 281–295.
- Roy, M., Jordan, T.H., Pederson, J., 2009. Colorado Plateau magmatism and uplift by warming of heterogeneous lithosphere. Nature 459 (7249), 978–982.
- Saleeby, J., 2003. Segmentation of the Laramide slab—evidence from the southern Sierra Nevada region. Geol. Soc. Am. Bull. 115 (6), 655–668.
- Stern, R.J., Gerya, T., 2018. Subduction initiation in nature and models: A review. Tectonophysics 746, 173–198.
- Tapponnier, P., Meyer, B., Avouac, J.P., Peltzer, G., Gaudemer, Y., Shunmin, G., Hongfa, X., Kelun, Y., Zhitai, C., Shuahua, C., Huagang, D., 1990. Active thrusting and folding in the Qilian Shan, and decoupling between upper crust and mantle in northeastern Tibet. Earth Planet. Sci. Lett. 97 (3–4), 382–403.
- Tarduno, J.A., McWilliams, M., Debiche, M.G., Sliter, W.V., Blake, M.C., 1985.
 Franciscan complex Calera limestones: Accreted remnants of Farallon plate oceanic plateaus. Nature 317 (6035), 345–347.
- Tharimena, S., Rychert, C.A., Harmon, N., 2016. Seismic imaging of a mid-lithospheric discontinuity beneath Ontong Java Plateau. Earth Planet. Sci. Lett. 450, 62–70.
- Tonegawa, T., Miura, S., Ishikawa, A., Sano, T., Suetsugu, D., Isse, T., Shiobara, H., Sugioka, H., Ito, A., Ishihara, Y., Tanaka, S., 2019. Characterization of crustal and uppermost-mantle seismic discontinuities in the Ontong Java Plateau. J. Geophys. Res. Solid Earth 124 (7), 7155–7170.
- van Hunen, J., van den Berg, A.P., Vlaar, N.J., 2000. A thermo-mechanical model of horizontal subduction below an overriding plate. Earth Planet. Sci. Lett. 182 (2), 157–169.
- van Hunen, J., Van Den Berg, A.P., Vlaar, N.J., 2002. On the role of subducting oceanic plateaus in the development of shallow flat subduction. Tectonophysics 352 (3–4), 317–333.
- van Hunen, J., van den Berg, A.P., Vlaar, N.J., 2004. Various mechanisms to induce present-day shallow flat subduction and implications for the younger Earth: a numerical parameter study. Phys. Earth Planet. Inter. 146 (1–2), 179–194.
- Wan, B., Wu, F., Chen, L., Zhao, L., Liang, X., Xiao, W., Zhu, R., 2019. Cyclical one-way continental rupture-drift in the Tethyan evolution: Subduction-driven plate tectonics. Sci. China Earth Sci. 1–12.

- Wang, T., Guo, L., Zhang, L., Yang, Q., Zhang, J., Tong, Y., Ye, K., 2015. Timing and evolution of Jurassic-cretaceous granitoid magmatisms in the Mongol-Okhotsk belt and adjacent areas, NE Asia: Implications for transition from contractional crustal thickening to extensional thinning and geodynamic settings. J. Asian Earth Sci. 97, 365–392.
- Windley, B.F., Maruyama, S., Xiao, W.J., 2010. Delamination/thinning of subcontinental lithospheric mantle under Eastern China: the role of water and multiple subduction. Am. J. Sci. 310 (10), 1250–1293.
- Wong, W.H., 1927. Crustal movements and igneous activities in Eastern China since Mesozoic time. 1. Bull. Geol. Soc. China 6 (1), 9–37.
- Wong, W.H., 1929. The Mesozoic orogenic movement in eastern China. Geol. Soc. China Bull. 8, 33–44.
- Wu, F., Xu, Y., Gao, S., Zheng, J., 2008. Lithospheric thinning and destruction of the North China Craton. Acta Petrol. Sin. 24, 1145–1170.
- Wu, F.Y., Yang, J.H., Wilde, S.A., Zhang, X.O., 2005. Geochronology, petrogenesis and tectonic implications of Jurassic granites in the Liaodong Peninsula, NE China. Chem. Geol. 221 (1–2), 127–156.
- Wu, F.Y., Li, X.H., Yang, J.H., et al., 2007. Discussions on the petrogenesis of granites (in Chinese). Acta Petrol. Sin. 23, 1217–1238.
- Wu, F.Y., Sun, D.Y., Ge, W.C., Zhang, Y.B., Grant, M.L., Wilde, S.A., Jahn, B.M., 2011. Geochronology of the Phanerozoic granitoids in northeastern China. J. Asian Earth Sci. 41 (1), 1–30.
- Wu, F.Y., Yang, J.H., Xu, Y.G., Wilde, S.A., Walker, R.J., 2019. Destruction of the North China craton in the Mesozoic. Annu. Rev. Earth Planet. Sci. 47, 173–195.
- Wu, Y.B., Zheng, Y.F., 2013. Tectonic evolution of a composite collision orogen: an overview on the Qinling-Tongbai-Hong'an-Dabie-Sulu orogenic belt in Central China. Gondwana Res. 23 (4), 1402–1428.
- Xiao, W., Windley, B.F., Hao, J., Zhai, M., 2003. Accretion leading to collision and the Permian Solonker suture, Inner Mongolia, China: termination of the central Asian orogenic belt. Tectonics 22 (6).
- Xu, W., Hergt, J.M., Gao, S., Pei, F., Wang, W., Yang, D., 2008. Interaction of adaktic melt-peridotite: implications for the high-Mg# signature of Mesozoic adaktic rocks in the eastern North China Craton. Earth Planet. Sci. Lett. 265 (1–2), 123–137.
- Xu, Y., Li, H., Pang, C., He, B., 2009. On the timing and duration of the destruction of the North China Craton. Chin. Sci. Bull. 54 (19), 3379.
- Xu, Y.G., 2001. Thermo-tectonic destruction of the Archaean lithospheric keel beneath the Sino-Korean Craton in China: evidence, timing and mechanism. Phys. Chem. Earth Solid Earth Geod. 26 (9–10), 747–757.
- Yang, J.H., Wu, F.Y., Wilde, S.A., Belousova, E., Griffin, W.L., 2008. Mesozoic decratonization of the North China block. Geology 36 (6), 467–470.
- Yin, A., Nie, S., 1993. An indentation model for the North and South China collision and the development of the Tan-Lu and Honam fault systems, eastern Asia. Tectonics 12 (4), 801–813.
- Yokoyama, K., Shigeoka, M., Otomo, Y., Tokuno, K., Tsutsumi, Y., 2016. Uraninite and thorite ages of around 400 granitoids in the Japanese Islands. Mem. Nation. Museum Nat. Sci. 51, 1–24.
- Zhai, M., Zhang, Y., Zhang, X., Wu, F., Peng, P., Li, Q., Hou, Q., Li, T., Zhao, L., 2016. Renewed profile of the Mesozoic magmatism in Korean Peninsula: Regional correlation and broader implication for cratonic destruction in the North China Craton. Sci. China Earth Sci. 59 (12), 2355–2388.
- Zhang, H.F., Goldstein, S.L., Zhou, X.H., Sun, M., Zheng, J.P., Cai, Y., 2008. Evolution of subcontinental lithospheric mantle beneath eastern China: Re–Os isotopic evidence from mantle xenoliths in Paleozoic kimberlites and Mesozoic basalts. Contrib. Mineral. Petrol. 155 (3), 271–293.
- Zhang, J., Zhao, Z.F., Zheng, Y.F., Dai, M., 2010b. Postcollisional magmatism: geochemical constraints on the petrogenesis of Mesozoic granitoids in the Sulu orogen, China. Lithos 119 (3–4), 512–536.
- Zhang, J.H., Gao, S., Ge, W.C., Wu, F.Y., Yang, J.H., Wilde, S.A., Li, M., 2010a. Geochronology of the Mesozoic volcanic rocks in the Great Xing an Range, northeastern China: implications for subduction-induced delamination. Chem. Geol. 276 (3–4), 144–165.
- Zheng, J., Dai, H., 2018. Subduction and retreating of the western Pacific plate resulted in lithospheric mantle replacement and coupled basin-mountain respond in the North China Craton. Sci. China Earth Sci. 61 (4), 406–424.
- Zheng, Y., Xu, Z., Zhao, Z., Dai, L., 2018. Mesozoic mafic magmatism in North China: Implications for thinning and destruction of cratonic lithosphere. Sci. China Earth Sci. 61 (4), 353–385.
- Zhi-qiang, F., Cheng-zao, J., Xi-nong, X., Shun, Z., Zi-hui, F., Cross, T.A., 2010. Tectonostratigraphic units and stratigraphic sequences of the nonmarine Songliao basin, Northeast China. Basin Res. 22 (1), 79–95.
- Zhong, X., Li, Z.H., 2020. Subduction initiation during collision-induced subduction transference: Numerical modeling and implications for the Tethyan evolution. J. Geophys. Res. Solid Earth 125 (2), e2019JB019288.
- Zhou, J.B., Li, L., 2017. The Mesozoic accretionary complex in Northeast China: evidence for the accretion history of Paleo-Pacific subduction. J. Asian Earth Sci. 145, 91–100.
- Zhou, Q., Liu, L., Hu, J., 2018. Western US volcanism due to intruding oceanic mantle driven by ancient Farallon slabs. Nat. Geosci. 11 (1), 70–76.
- Zhou, X.M., Li, W.X., 2000. Origin of late Mesozoic igneous rocks in Southeastern China: implications for lithosphere subduction and underplating of mafic magmas. Tectonophysics 326 (3–4), 269–287.
- Zhu, R., Xu, Y., 2019. The subduction of the West Pacific plate and the destruction of the North China Craton. Sci. China Earth Sci. 1–11.
- Zhu, R., Xu, Y., Zhu, G., Zhang, H., Xia, Q., Zheng, T., 2012. Destruction of the North China craton. Sci. China Earth Sci. 55 (10), 1565–1587.